HHS Public Access

Author manuscript

Cancer Res. Author manuscript; available in PMC 2019 February 15.

Published in final edited form as:

Cancer Res. 2018 February 15; 78(4): 891–908. doi:10.1158/0008-5472.CAN-17-2353.

Oncogenic RAS-Induced Perinuclear Signaling Complexes Requiring KSR1 Regulate Signal Transmission to Downstream Targets

Sandip K. Basu[1], **Sook Lee**[1], **Jacqueline Salotti**[1], **Srikanta Basu**[1], **Krisada Sakchaisri**[1], **Zhen Xiao**[2], **Vijay Walia**[3], **Christopher J. Westlake**[3], **Deborah K. Morrison**[3], and **Peter F. Johnson**[1,*]

[1]Mouse Cancer Genetics Program, Center for Cancer Research, National Cancer Institute, Frederick, MD, 21702 USA

[2]Laboratory of Proteomics and Analytical Technologies, Leidos Biomedical Research, Inc., Frederick National Laboratory for Cancer Research, Frederick, MD, 21702 USA

[3]Laboratory of Cell and Developmental Signaling, Center for Cancer Research, National Cancer Institute, Frederick, MD, 21702 USA

Abstract

The precise characteristics that distinguish normal and oncogenic RAS signaling remain obscure. Here we show that oncogenic RAS and BRAF induce perinuclear re-localization of several RAS pathway proteins, including the kinases CK2 and p-ERK1/2 and the signaling scaffold KSR1. This spatial reorganization requires endocytosis, the kinase activities of MEK-ERK and CK2, and the presence of KSR1. CK2α co-localizes with KSR1 and Rab11, a marker of recycling endosomes, whereas p-ERK associates predominantly with a distinct KSR1-positive endosomal population. Notably, these perinuclear signaling complexes (PSCs) are present in tumor cell lines, mouse lung tumors and mouse embryonic fibroblasts undergoing RAS-induced senescence. PSCs are also transiently induced by growth factors (GFs) in non-transformed cells with delayed kinetics (4–6 hr), establishing a novel late phase of GF signaling that appears to be constitutively activated in tumor cells. PSCs provide an essential platform for RAS-induced phosphorylation and activation of the pro-senescence transcription factor C/EBPβ in primary MEFs undergoing senescence. Conversely, in tumor cells C/EBPβ activation is suppressed by 3′UTR-mediated localization of *Cebpb* transcripts to a peripheral cytoplasmic domain distinct from the PSC region. Collectively, our findings indicate that sustained PSC formation is a critical feature of oncogenic RAS/BRAF signaling in cancer cells that controls signal transmission to downstream targets by regulating selective access of effector kinases to substrates such as C/EBPβ.

[*]**Corresponding author:** Peter F. Johnson, Mouse Cancer Genetics Program, Center for Cancer Research, National Cancer Institute, Frederick, MD, 21702 USA johnsope@mail.nih.gov.

Present addresses: **Krisada Sakchaisri:** Department of Pharmacology, Faculty of Pharmacy, Mahidol University, Bangkok, Thailand

Present addresses: **Vijay Walia:** Division of Genetic and Molecular Toxicology, National Center for Toxicological Research, US Food and Drug Administration, Jefferson, AR, 72079 USA

The authors declare no potential conflicts of interest.

Introduction

RAS GTPases play pivotal roles in transducing extracellular growth factor (GF) signals to downstream pathways. *RAS* proto-oncogenes are among the most frequently mutated in cancer, with ~30% of human and rodent tumors carrying *RAS* lesions (1). *RAS* cancers are particularly aggressive and resistant to treatment and are associated with poor clinical outcomes. Oncogenic mutations stabilize the active GTP-bound form of RAS, resulting in continuous GF-independent signaling, primarily through the RAF-MEK-ERK (MAPK) pathway. The prevalence of *RAS* mutations in cancer has prompted extensive efforts to define the properties that distinguish mutant RAS signaling from that elicited by GFs. Oncogenic RAS signaling is often characterized by strong effector pathway activation, particularly through the MAPK cascade, and sustained duration (2). By contrast, GF-induced signal transduction is constrained by feedback regulators that attenuate RAS-ERK activation (3), and these controls are absent or curtailed in *RAS* tumor cells. Although normal and pathological RAS signaling have been studied extensively, a full understanding of the features that underlie “oncogenic drive” by mutant RAS is still lacking. For example, cancer cells do not always exhibit elevated MAPK pathway output despite the presence of mutations such as *KRAS* that are expected to activate the RAF-MEK-ERK cascade (The Cancer Genome Atlas Research Network, 4,5). These observations suggest that additional properties besides RAS-ERK amplitude may be required for neoplastic transformation.

In addition to its oncogenic activity in cancer cells, expression of mutant RAS in normal primary cells can provoke oncogene-induced senescence (OIS), a permanent form of cell cycle arrest that provides an intrinsic barrier to tumorigenesis (6-8). Senescence typically involves induction of the Arf-p53 and $p16^{Ink4a}$-Rb tumor suppressor pathways. The transcription factor C/EBPβ has also emerged as an important effector of *RAS*- and *BRAF*-induced senescence in primary fibroblasts. *Cebpb*$^{-/-}$ MEFs or *CEBPB*-depleted human fibroblasts do not undergo OIS and display impaired expression of senescence-associated secretory phenotype (SASP) genes (9-12), which are typically up-regulated in senescent cells (13,14). Oncogenic RAS induces post-translational activation of C/EBPβ, which otherwise is maintained in an auto-inhibited, low activity state (15-18). The activated form of C/EBPβ is cytostatic, recruits p300/CBP coactivators and activates SASP genes (9,18). C/EBPβ can also be transiently activated by normal GF signals. C/EBPβ de-repression is critically dependent on the RAF-MEK-ERK cascade, and several RAS–induced modifications mediate increased DNA binding, transcriptional activity and homodimerization (18). C/EBPβ is directly phosphorylated by ERK on Thr188 (19), although this modification is dispensable for RAS-induced DNA binding (18). In addition, phosphorylation on C/EBPβ Ser273 in the leucine zipper by the ERK-activated kinase, $p90^{RSK}$, potentiates DNA binding and homodimerization and is critical for its cytostatic activity (18).

We previously reported that C/EBPβ activation by $HRAS^{G12V}$ signaling is suppressed in immortalized/transformed cells by the 3′ untranslated region (3′UTR) of its mRNA (20). This novel mechanism, termed “3′UTR regulation of protein activity” (UPA), depends on 3′UTR-mediated localization of *Cebpb* transcripts to the peripheral cytoplasm. In this location, newly-synthesized C/EBPβ is inaccessible to its activating kinase, p-ERK1/2,

which is confined to a distinct perinuclear region of the cytoplasm. This spatial separation from p-ERK, and potentially other kinases, suppresses C/EBPβ activation in tumor cells and prevents it from inducing growth arrest, senescence and SASP genes. Importantly, UPA is not observed in primary cells such as MEFs that undergo OIS (20). In these cells, endogenous C/EBPβ expressed from the native 3′UTR-containing transcript can be activated by oncogenic RAS signaling and *Cebpb* transcripts are uniformly localized in the cytoplasm. Thus, UPA disengages C/EBPβ from RAS signaling specifically in tumor cells, facilitating senescence bypass.

Here, we have assessed the subcellular localization of several RAS pathway proteins and the role of such compartmentalization in regulating signal transmission to C/EBPβ. We show that perinuclear signaling complexes (PSCs), which are localized structures containing multiple RAS pathway components, are induced persistently or transiently by mutant and physiological RAS signaling, respectively. Disruption of PSCs blocked RAS-C/EBPβ signaling. Furthermore, sustained PSC formation was observed in all tumor cells examined, indicating a critical function for localized RAS signaling in neoplastic transformation. Our studies provide new insights into the spatial organization of RAS pathway kinases and highlights their involvement in controlling post-translational activation of a downstream effector.

Materials and Methods

Animals and preparation of MEFs

Mice were maintained in accordance with National Institutes of Health animal guidelines following protocols approved by the NCI-Frederick Animal Care and Use Committee. Mouse embryonic fibroblasts (MEFs) were isolated from *WT* and $KSR1^{-/-}$ E13.5 mouse embryos (21) and were maintained at low passage without immortalization. $Kras^{LA2/+}$ mice (22) were aged to allow spontaneous development of lung tumors. Ad.Cre virus (Viral Vector Core Facility, University of Iowa College of Medicine) was administered to *LSL-*$BRAF^{V600E/+}$ animals (23) by intratracheal instillation (7.5×10^6 Pfu/animal) to induce lung tumors.

Cells and cell culture

A549, A375, HEK-293T, HeLa, MDA-MB-231, RKO, and HepG2 cells (American Type Culture Collection, Rockville, MD) and 293GP2 packaging cells (ATTC) were cultured in DMEM (Gibco) supplemented with 10% FBS (Gibco). MCF10a cells (ATCC) were cultured in DMEM supplemented with Horse Serum (5%), EGF (20ng/ml), Hydrocortisone (0.5 mg/ml), Cholera Toxin (100 ng/ml) and Insulin (10 μg/ml). MIA PaCa-2 cells (ATCC) were cultured in DMEM with 10% fetal bovine serum and 2.5% horse serum (Gibco). SW-1573 cells (ATCC) were grown in RPMI-1640 (Gibco) with 10% fetal bovine serum. NIH3T3 and $3T3^{RAS}$ cells were grown in DMEM with 10% calf serum (Colorado Serum Company). All media were supplemented with Normocin (InvivoGen) to prevent Mycoplasma contamination. Cell lines were not authenticated. Cells were generally passaged fewer than 5 times, and freshly thawed cells were maintained in culture for no more than two weeks before conducting experiments. For serum starvation, cells were plated and cultured for 24

hr, the media was replaced by DMEM containing 0.1% serum for 24 hr, after which the cells were stimulated with 10% serum and harvested at the indicated time points.

Antibodies and reagents

Affinity-purified rabbit antibody to Rab11 (D4F5), p-ERK (197G2) and phospho-C/EBPβ (T235/T188, #3084) were purchased from Cell Signaling Technologies. Rabbit antibodies to C/EBPβ (C-19), ERK1 (C-19), CK2α (H-286), KSR-1 (H-70), BRAF (H-145) and actin (I-19-R), and mouse antibodies to CK2α (E-7), p-ERK (E-4), p-Elk-1 (B-4) and BRAF (F-7) were purchased from Santa Cruz Biotechnology. Rabbit antibody to HRAS (GTX-116041) was from GeneTex. Mouse antibodies to Rab11 and RAS (panRAS) were from BD Biosciences. Affinity purified mouse antibody against Pyo epitope tag (Glu-Glu) was purchased from BioLegend. Anti-mouse (W4028) and anti-rabbit (W4018) HRP conjugated secondary antibodies were from Promega. Anti-Mouse Alexa® Fluor 488 and anti-rabbit Alexa® Fluor 594 conjugated secondary antibody was from Thermo. An anti-phospho-Ser222/223 antibody was raised in rabbits using the following immunogenic peptide: (NH_2-Cys-Lys-Ala-Val-Asp-Lys-Leu-P-Ser-Asp-Glu-Tyr-Lys). The N-terminal Cys was added for coupling to KLH and the C-terminal Lys was amidated. The antiserum was purified by affinity binding to the phosphorylated peptide and absorbed against the non-phosphorylated peptide.

FuGENE6 and X-tremeGENE HP DNA transfection reagents were from Roche Diagnostics. Inhibitors, including dynasore hydrochloride (Santa Cruz), TBB (Sigma), CX-4945 (Activate Scientific), U0126 (Promega) and SCH772984 (MedChem Express), were reconstituted following the manufacturer's recommendations and used at the indicated doses. ON-Target Plus Smart Pool siRNA against mouse CK2α (L-058353-00 and L-051582-00), and KSR-1 (L-045873-00) and a non-silencing control siRNA (D-001810-10) were purchased from Dharmacon (Thermo Scientific). CK2 holoenzyme was purchased from SignalChem. Primers used in RT-qPCR analysis were from Qiagen: *Il-6* (QT00098875), *Il1a* (QT00113505), *Cxcl1* (QT00115647), *Cxcl2* (QT00113253), *Ccr1* (QT00156058) and *Pp1a* (QT00247709).

Plasmids

Expression plasmids for the mouse C/EBPβ coding region (C/EBPβ$^{\Delta UTR}$) and C/EBPβ coding region plus 3′UTR (C/EBPβ^{UTR}) were previously described (20); the inserts were also transferred to pBabe-puro. Lentiviral expression vectors for GFP-tagged mouse KSR1 and mCherry-tagged mouse CK2α were purchased from Genecopia (Rockville, MD). Human and mouse KSR1-specific shRNA and a non-targeting control shRNA in the pLKO.1-Puro lentiviral vector have been described (24). Plasmid and retroviral vectors for human HRAS^{G12V} have been described (11). Mouse C/EBPβ mutant plasmids (S223A and S223D) were generated using a Stratagene site-directed mutagenesis kit per the manufacturer's instructions. Retroviral packaging plasmid, VSVG, was a gift from S. Hughes, and lentiviral packaging/envelope plasmids pMD2.G (#12259), pMDLg/pRRE (#12251), and pRSV/Rev (#12253) were purchased from AddGene.

Retroviral vectors and virus infection

Retroviral and lentiviral plasmids were transfected into 293GP2 and 293T packaging cell lines, respectively, using a standard $CaPO_4$ precipitation method. For lentiviral transfection, 20 μg of lentiviral vector, 6 μg of pMD2.G, 10 μg of pMDLg/pRRE and 5 μg of pRSV/Rev were co-transfected into 293T cells. For retroviral transfection, 20 μg of retroviral vector and 4 μg of VSVG plasmid were co-transfected into 293GP2 cells in 10 cm dishes. 48–72 hr after transfection, viral supernatants were collected every 12 h, pooled, filtered (0.45 mm), supplemented with 8 mg/ml polybrene, and used to infect target cells. Three infections were performed, after which the cells were selected in appropriate antibiotics. Multiple genes were introduced by sequential infection and drug selection.

Colony assays and growth curves

For colony assays, MEFs were seeded at 2.5×10^4 cells/dish in 10 cm dishes. Media was replaced weekly. After two weeks, cells were washed with phosphate-buffered saline (PBS), fixed in 10% acetic acid for 30 min, rinsed with water, stained with 0.4% crystal violet (Sigma) for 30 min, rinsed extensively, and dried. For growth curves, cells were seeded at 2.5×10^4 cells/well in 6-well dishes. At the appropriate times, cells were washed with phosphate-buffered saline (PBS), fixed in 10% formalin, rinsed with water, stained with 0.1% crystal violet (Sigma) for 30 min, rinsed extensively, and dried. Dye was then extracted with 10% acetic acid and absorbance measured at 590 nm. All values were normalized to day 0 (the first day after plating).

Transient transfection

Transfections were carried out using 50–60% confluent cell monolayers in 60mm tissue culture dishes using FuGENE6 or X-treme GENE HP (Roche) reagents per the manufacturer's instructions. HEK293T cells were transfected with 200 ng C/EBPβ vector and 100 ng of pcDNA3-$HRAS^{G12V}$ in 60mm dishes. After transfection, cells were cultured in complete media for 24h and serum starved overnight prior to harvesting. Where applicable, specific inhibitors were added at the time of starvation. For all experiments, the total amount of DNA (1.0 μg per 60mm dish) was kept constant by adding an appropriate amount of the empty plasmid.

Luciferase assays

For transactivation assays, 293T cells were transfected with 100 ng 2X C/EBP-luc reporter and 5 ng C/EBPβ vector with 10 ng $HRAS^{G12V}$ plasmid. Cells were lysed in 1X passive lysis buffer (Promega) and luciferase activity was measured using a GLOMAX 20/20 luminometer (Promega). Luciferase values were normalized to total protein concentration of the lysate. Data are presented as fold activation over the reporter alone and represent means ± SD of at least three independent experiments.

Identification of C/EBPβ phospho-modifications by mass spectrometry

Rat C/EBPβ (HA-tagged LAP isoform) was expressed in 293T cells together with $HRAS^{G12V}$, immunoprecipitated and analyzed by mass spectrometry as described previously (18).

Expression and purification of recombinant C/EBPβ proteins

Full length and truncated rat C/EBPβ proteins were expressed in *E. coli* and purified as described previously (17).

Immunoblotting

Cells were harvested after washing twice with cold PBS and lysed with low salt buffer (20mM HEPES of pH 7.9, 0.1mM EDTA, 10mM NaCl, 0.1% NP-40) on ice for 10 min. Nuclei were harvested by centrifugation at 3500 rpm for 10 min, and the supernatant was used as cytoplasmic fraction. Nuclei were lysed with high salt buffer (20 mM HEPES pH 7.9, 0.2 mM EDTA, 420 mM NaCl, 25% glycerol) at 4°C for 30 min with vigorous shaking. Nuclear debris was pelleted by centrifugation at 14,000 rpm for 5 min, and the supernatant was used for further experiments or stored at −70°C. All buffers were supplemented with a protease and phosphatase inhibitor cocktail (Calbiochem). Protein samples (20-50μg) were resolved by electrophoresis on 10% or 12% Mini-PROTEAN TGX Precast Gels (Biorad) and electrophoretically transferred to PVDF membranes. The blots were probed with the appropriate primary antibodies followed by goat anti-rabbit IgG or goat anti-mouse IgG conjugated to horseradish peroxidase and visualized using enhanced chemiluminescence (Thermo Scientific).

Electrophoretic mobility shift assays (EMSAs)

EMSA was performed essentially as described (25). The dsDNA probe containing a consensus C/EBP site was end-labeled with polynucleotidylkinase (Roche) and [^{32}P]dATP (Amersham). DNA-binding assays were carried out in a 25 μl reaction containing nuclear extract (5 to 10 μg), 20 mM HEPES (pH 7.9), 200 mM NaCl, 5% Ficoll, 1 mM EDTA, 50 mM DTT, 0.01% Nonidet P-40, 1.75 μg of poly(dI-dC), and 2×10^4 cpm probe. After incubation for 20 min at room temperature, 10-15 μl of the binding reaction was loaded onto a 6% polyacrylamide gel in TBE (90 mM Tris base, 90 mM boric acid, 0.5 mM EDTA) buffer and electrophoresed at 160 V for 2 h. Supershift assays were carried out by pre-incubating the nuclear extract with 1 μl of appropriate antibody at 4°C for 30 min before addition of the binding reaction mixture.

Senescence-associated β-galactosidase assays—MEFs (passage 2-4) were infected with a HRAS^{G12V}-expressing retrovirus or control vector and, after selection, plated at 5×10^4 cells per well in 6-well plates and cultured for 3-4 days. Cells were fixed and stained (Senescence Detection Kit; Calbiochem) according to the manufacturer's instructions except that the staining solution was titrated with 2M HCl to ensure the pH was less than 6.0. SA-β-gal stained cells were counted by acquiring at least four fields using 10x bright field microscopy. Data are expressed as a percentage of the total cells scored.

Immunofluorescence

For immunofluorescence of cultured cells, 2.5×10^4 cells were plated in glass-bottomed chambers (LabTek) and cultured for 24 hrs. Cells were serum starved overnight prior fixation and, when applicable, treated with specific inhibitors overnight before fixation. Cells were fixed with ice cold methanol for 20 min at −20°C, blocked for 1 hr in PBS with

5% Normal Goat Serum (Cell Signaling) and 0.1% TritonX100 (Sigma), and incubated with the appropriate primary antibodies (1:100) overnight at 4°C in blocking buffer. Following four washes with PBS containing 1% BSA and 0.1% TritonX100, cells were incubated with Alexa 488 and Alexa 594 conjugated secondary antibodies (1:1000) for 1 hr. at RT. After five washes cells were stained with 0.1 μg/mL DAPI in PBS for 15 min at RT followed by two washes with PBS. Fluorescence images were acquired using a Zeiss LSM-710 confocal microscope. For tumor samples, dissected lungs from $Kras^{LA2}$/+ mice and $LSL\text{-}BRAF^{V600E}$/+ animals were fixed overnight in 4% paraformaldehyde, after which OCT embedded frozen blocks were prepared. 10 μm sections were made, fixed again in ice-cold methanol for 10 min at −20°C and permeabilized with 1% TritonX100 for 15 min at RT and 1% SDS for 5 min at RT; all steps were interspersed with three PBS washes. The blocking steps and staining with primary and secondary antibodies and DAPI were performed as described above.

mRNA localization

The GFP-MS2-nls reporter system and pcDNA-$Cebpb^{\Delta UTR}$-Ms2b and pcDNA-$Cebpb^{UTR}$-Ms2b constructs have been described previously (20,26). NIH3T3 cells were plated at 5×10^4 cells/35mm dish and transfected with 200 ng GFP-MS2-nls reporter plasmid and 2.3 μg of the *Cebpb*-Ms2b vector using Polyfect (Qiagen), following the manufacturer's recommendations. After 36 hr, the cells were fixed with 4% PFA in PBS for 20 min at room temperature and then blocked with 5% normal goat serum. The cells were stained with primary antibody against CK2α and Alexa 594 conjugated secondary antibody, followed by DAPI staining as described above. Fluorescence images were taken with a Zeiss LSM-710 confocal microscope.

RNA fluorescence *in situ* hybridization and immunofluorescence (FISH-IF)

Twelve thousand NIH3T3 cells or 2×10^4 human tumor cells were plated on μ-Slides $VI^{0.4}$ (Ibidi). Forty-eight hr after seeding, cells were washed in Cytoskeleton Buffer (CB) (27) (10 mM MES pH 6.1, 150 mM NaCl, 5 mM $MgCl_2$, 5 mM EGTA, 5 mM glucose) and permeabilized/fixed in ice-cold Pre-Fixative mix (28) (2% paraformaldehyde, 0.01% glutaraldehyde, 0.05% saponin, in CB) for 15 min at 4°C. Cells were then incubated with ice-cold Fixative mix (2% paraformaldehyde, 0.01% glutaraldehyde, in CB) for 100 min at 4°C. Fixed cells were washed with CB twice and quenched by addition of 50 mM NH_4Cl for 5 min at 20°C. For FISH, QuantiGene ViewRNA ISH Cell Assay (Affymetrix) was used according to the manufacturer's protocol; a human *CEBPB* FISH probe was used for hybridization (VA1-18129). Cells were then blocked with 5% albumin in PBS-S (0.05% Saponin, in PBS) for 1 hr at 20°C and incubated with CK2α primary antibody (1:100) for 16 hr at 4°C in 5% albumin in PBS-S. Cells were washed three times for 5 min at 20°C with PBS-S and incubated for 1 hr at 20°C with Alexa 488 and Alexa 647 conjugated secondary antibodies (1:1000) in 5% albumin/PBS-S. Cells were washed four times with PBS-S for 5 min at 20°C, co-stained with 0.1 μg/mL DAPI (in PBS) for 1 min at 20°C and then washed twice with PBS. Images were acquired using a Zeiss LSM-780 confocal microscope.

siRNA transfection

A375 melanoma cells (homozygous *BRAF*^{V600E}) were transfected with 100 nM BRAF^{V600E} siRNA (sense: 5′-GCUACAGAGAAAUCUCGAUUU; antisense: 5′-AUCGAGAUUUCUCUGUAGCUU). NIH3T3 cells were transfected with 100 nM KSR1, CK2α, or non-silencing control siRNAs. All siRNAs were transfected using DharmaFECT 1 (Dharmacon). Whole cell lysates were prepared 48 hr after transfection.

Reverse transcription and quantitative PCR (RT-qPCR)

Total RNA was extracted with GeneJet RNA Purification kit (Thermo) and reverse transcribed using Maxima First Strand cDNA Synthesis kit (Thermo) according to the manufacturer's protocol. Quantitative PCR using SsoAdvanced SYBR Green Supermix (Bio-Rad) was performed using CFX96 Real Time PCR System (Bio-Rad). Ppia was used as a normalization reference gene. Primers are listed under **Antibodies and Reagents**.

Immunoprecipitations

1×10^6 HEK293T cells were seeded in 10 cm dishes and transfected with 4 μg pcDNA3-pyo-KSR1 vector with or without 0.5 μg pcDNA3-HRAS^{G12V} vector, or left untransfected. Transfection was carried out using FuGENE6 (Promega) as described above. 24 hr after transfection, the cells were serum starved overnight, with or without inhibitors as indicated (5 μM U0126, 10 μM TBB, or 40 μM dynasore). The cells were harvested and lysed in Lysis Buffer (137 mM NaCl, 20 mM Tris pH 8.0, 10% glycerol and 1% NP40). The lysates were centrifuged at 13,000 rpm for 5 minutes and the supernatants were collected. Protein estimation was performed using Bradford's reagent (Bio-Rad), and 1600 μg of the supernatant was used for immunoprecipitation. 3% of each supernatant was reserved for input samples. Anti-pyo antibody (1:100) was added to the supernatants and incubated for 3 hr at 4°C on a rotating rack. Thereafter, 30μl of a 50% slurry of Protein G sepharose was added and incubated at 4°C on a rotating rack for 1 hr. The beads were pelleted by centrifugation at 3000 rpm for 1 minute and washed 4 times in Wash Buffer (5 M NaCl, 20 mM Tris pH 8.0, 1 mM EDTA and 0.5% NP40). 2xSDS sample buffer (Bio-Rad) was added to the beads and the samples boiled for 8 minutes at 100°C. The proteins were analyzed by immunoblotting as described above.

Statistical analysis

Statistical significance was calculated using Student's t test and ANOVA. P values less than 0.05 were considered significant.

Results

C/EBPβ Ser222 is a CK2 phosphoacceptor that controls C/EBPβ activation by RAS signaling

To extend our understanding of C/EBPβ activation by oncogenic RAS and its inhibition by the 3′UTR mechanism, we sought to identify additional modifications that regulate C/EBPβ activity. We previously used ^{32}P-phosphopeptide mapping and mass spectrometry to identify several RAS-induced PTMs on C/EBPβ (18). Further analysis of these data showed that

Ser223 in rat C/EBPβ (Ser222 in mouse) was also consistently phosphorylated when the protein was co-expressed with $HRAS^{G12V}$ (Fig. 1A and Supplementary Fig. S1A). Ser223/222 is located within the extended basic region, indicting a possible role in DNA binding. Using EMSA to assess DNA binding of WT and mutant C/EBPβ proteins expressed from constructs lacking the 3′UTR ($C/EBP\beta^{\Delta UTR}$) in 293T cells, we found that a phosphorylation-defective variant (S223A) was refractory to activation by $HRAS^{G12V}$ while a phosphomimetic mutant (S223D) displayed elevated basal binding (Fig. 1B). Transactivation assays using a C/EBP-driven reporter (2X C/EBP-luc) showed that RAS-stimulated C/EBPβ transcriptional activity was impaired in the S223A mutant and increased for S223D (Fig. 1C). Furthermore, stable expression of WT C/EBPβ in $HRAS^{G12V}$–expressing *Cebpb*$^{-/-}$ MEFs caused proliferative arrest, whereas the S223A mutant displayed impaired cytostatic activity in colony formation assays (Fig. 1D) and growth assays (Supplementary Fig. S1B). Thus, this residue plays a significant role in regulating C/EBPβ activity in the context of RAS signaling.

The presence of conserved acidic residues at positions N+1 and N+2 (Fig. 1A) suggested that Ser223 may be a CK2 site (29). Accordingly, incubation of recombinant rat C/EBPβ with CK2 holoenzyme and ATP stimulated its DNA-binding activity (Fig. 1E) and catalyzed phosphorylation on Ser223, as determined by deletion mapping and MS analysis (Supplementary Fig. S1C-D). Furthermore, treatment of cells with the CK2 inhibitor 4,5,6,7-tetrabromo-2-azabenzimidazole (TBB) blocked RAS-induced augmentation of C/EBPβ DNA-binding (Fig. 1F) and transcriptional activity (Fig. 1G). Using an antibody raised against C/EBPβ phospho-Ser223, we detected a weak basal p-Ser223 signal for WT C/EBPβ that was strongly increased by co-expression of $HRAS^{G12V}$ (Fig. 1F, lower panel), whereas C/EBPβ S223A was not recognized by the antibody (Supplementary Fig. S1E). RAS-induced phosphorylation on Ser223 was also blocked by TBB (Fig. 1F, lane 3). TBB similarly inhibited DNA binding of endogenous C/EBPβ in $HRAS^{G12V}$-expressing MEFs and decreased phosphorylation on Ser222 (Fig. 1H). Finally, co-IP assays showed that HA-tagged C/EBPβ interacted with endogenous CK2α in 293T cells and this association was enhanced by co-expression of oncogenic RAS (Fig. 1I). Thus, RAS signaling stimulates the interaction between C/EBPβ and its upstream kinase, CK2.

We also investigated whether RAS-induced transcription of C/EBPβ target genes requires CK2 activity. We previously showed that C/EBPβ expressed from the $C/EBP\beta^{\Delta UTR}$ construct potently activates transcription of SASP genes in $NIH3T3^{RAS}$ cells ($\beta^{\Delta UTR}$-$3T3^{RAS}$ cells) (20). As shown in Fig. 1J, siRNA depletion of CK2α (catalytic subunit) in these cells reduced the levels of IL-6, IL-1α, Cxcl1, Cxcl2, and Ccr1 mRNAs by 40-60%. Thus, CK2 is required for efficient C/EBPβ-dependent transcription of SASP genes. TBB and another CK2 inhibitor, CX-4945 (30), also efficiently suppressed $HRAS^{G12V}$-induced senescence in MEFs as determined by senescence-associated β-galactosidase staining (Fig. 1K). Collectively, the data of Fig. 1 show that CK2-mediated phosphorylation on Ser222 is critical for induction of C/EBPβ DNA-binding and cytostatic activity and its ability to activate SASP genes.

CK2 undergoes HRAS^{G12V}-induced perinuclear re-localization, allowing UPA-mediated inhibition of Ser222 phosphorylation

We next investigated whether phosphorylation on C/EBPβ Ser222 is blocked by the *Cebpb* 3′UTR. As shown in Fig. 2A, the *Cebpb* 3′UTR suppressed RAS-induced phosphorylation of Ser222 in 293T cells; ERK-mediated phosphorylation on T188 was also inhibited, supporting our previous findings (20). The abrogation of Ser222 phosphorylation by the UPA mechanism suggested that CK2 might access C/EBPβ exclusively in the perinuclear region. Immunofluorescence imaging of CK2α in non-transformed NIH3T3 cells showed nuclear staining as well as diffuse cytoplasmic signals (Fig. 2B, left panels). However, expression of HRAS^{G12V} caused perinuclear re-localization of CK2α, with only faint staining remaining in the nucleus. This perinuclear compartmentalization was similar to that seen for p-ERK (Fig. 2B, right panels). A CK2α-mCherry fusion protein showed the same RAS-induced re-localization in live (unfixed) cells (Fig. 2C), supporting the IF results. Since CK2 is reported to have constitutive kinase activity, these findings indicate that the inducible phosphorylation observed for C/EBPβ expressed from the *Cebpb*$^{\Delta UTR}$ construct involves altered compartmentalization of CK2.

We also used MS2-GFP mRNA tagging to visualize *Cebpb*^{UTR} transcripts in 3T3^{RAS} cells, together with IF staining of CK2α, to determine if they show mutually exclusive localization. As observed previously (20), transcripts containing the 3′UTR were polarized toward the cell periphery, while those containing only the coding region showed uniform cytoplasmic distribution (Fig. 2D). CK2α was present mainly in the perinuclear cytoplasm and was concentrated in areas devoid of *Cebpb*^{UTR} mRNA. We confirmed these results using RNA FISH to visualize endogenous *CEBPB* transcripts, together with CK2α immunostaining, in human PANC-1 pancreatic tumor cells (mutant *KRAS*). *CEBPB* mRNAs were specifically excluded from a nuclear-proximal region that was typically positioned asymmetrically on one side of the nucleus (Fig. 2E). In contrast, CK2α was highly concentrated in the area devoid of *CEBPB* transcripts. Similar patterns were seen for MIA PaCa-2 cells (pancreatic carcinoma; *KRAS*^{G12C}) and SW-1573 cells (lung alveolar cell carcinoma; *KRAS*^{G12C}) (Fig. 2E). These findings support the notion that RAS-induced phosphorylation of C/EBPβ by CK2 occurs in a perinuclear location and can be inhibited in tumor cells by 3′UTR-dependent *Cebpb* mRNA trafficking to a non-overlapping region.

The MAPK scaffold KSR1 is required for perinuclear localization of p-ERK and CK2

Since perinuclear sorting of p-ERK and CK2 appears to be critical for their ability to phosphorylate C/EBPβ in a 3′UTR (UPA)-regulated manner, we sought to determine how p-ERK and CK2 are restricted to the perinuclear region. We hypothesized that the signaling scaffold, KSR1, may play a key role, as it has been shown to interact with both p-ERK and CK2 (31). Moreover, KSR1 is required for both RAS-induced transformation and OIS in mouse fibroblasts (32,33). We first asked whether C/EBPβ DNA binding requires KSR1. HRAS^{G12V} strongly augmented C/EBPβ DNA binding in *WT* MEFs but this response was severely curtailed in *KSR1*$^{-/-}$ cells (Fig. 3A). Expression of SASP genes was also strongly reduced in the mutant cells (Fig. 3B), correlating with impaired C/EBPβ DNA binding. IF imaging revealed that KSR1 in MEFs was broadly distributed in the cytoplasm but became

localized in a perinuclear ring upon expression of oncogenic RAS (Fig. 3C). Thus, KSR1 translocates to the perinuclear region in primary MEFs undergoing OIS.

Since KSR1 is required for C/EBPβ activation by RAS, we tested whether KSR1 and C/EBPβ physically interact by performing IP assays using Pyo-tagged KSR1 expressed in 293T cells. As shown in Fig. 3D (lanes 3 and 4), C/EBPβ$^{\Delta UTR}$ co-immunoprecipitated with KSR1 and this interaction was increased in cells expressing HRAS^{G12V}. However, the interaction of C/EBPβ^{UTR} with KSR1 was significantly reduced (lanes 5 and 6) compared to C/EBPβ$^{\Delta UTR}$, despite similar levels of C/EBPβ expressed from the two constructs. Thus, C/EBPβ associates with KSR1, either directly or indirectly, in a RAS-stimulated manner and this interaction is inhibited by the *Cebpb* 3′UTR, which directs *Cebpb* transcripts away from the perinuclear region. These data suggest that C/EBPβ must be translated in the perinuclear compartment to efficiently bind to KSR1.

CK2α and p-ERK also became perinuclear in MEFs expressing HRAS^{G12V} (Fig. 3E). This RAS-induced localization requires KSR1, as perinuclear targeting of the two kinases was disrupted in *KSR1*$^{-/-}$ cells. p-ERK levels were also reduced in the RAS-expressing mutant cells, consistent with the known function of KSR1 in facilitating signaling through the RAS-ERK cascade (3). Conversely, p-ERK was modestly increased in control *KSR1*$^{-/-}$ MEFs relative to *WT* cells, an effect that can be attributed to loss of KSR1-mediated, ERK-dependent negative feedback on RAF and MEK activity (34). Thus, CK2α and p-ERK are restricted to a nuclear proximal region in MEFs undergoing RAS-induced senescence in a manner that depends on KSR1.

C/EBPβ$^{\Delta UTR}$-expressing NIH3T3^{RAS} cells show activation of C/EBPβ DNA binding due to loss of 3′UTR inhibition (20). siRNA-mediated ablation of KSR1 in these cells reduced C/EBPβ DNA binding (Supplementary Fig. S2A), correlating with diminished expression of SASP genes (Supplementary Fig. S2B). In addition, endogenous KSR1 and an ectopic GFP-KSR1 chimeric protein both re-localized to the perinuclear cytoplasm in NIH3T3^{RAS} cells compared to non-transformed NIH3T3 controls (Supplementary Fig. S2C-D and Fig. 3F). KSR1 also colocalized substantially with CK2α and p-ERK in the RAS-expressing cells. KSR1 depletion disrupted perinuclear localization of CK2α and p-ERK in NIH3T3^{RAS} cells (Supplementary Fig. S2C-D), paralleling the effect seen in *KSR1*$^{-/-}$ MEFs. These data show that KSR1 plays a key role in the perinuclear trafficking of these effector kinases in response to oncogenic RAS, irrespective of whether the cells undergo senescence (MEFs) or transformation (NIH3T3 cells).

Perinuclear signaling complexes (PSCs) are common features of tumor cells and require MEK-ERK and CK2 activity

We next sought to extend our findings to tumor cell lines carrying endogenous RAS pathway oncogenes. We first examined A549 cells, which are derived from a human *KRAS*^{G12C}–containing lung adenocarcinoma. p-ERK, CK2α and KSR1 were present in discrete, ring-like perinuclear structures in A549 cells, and KSR1 co-localized with both CK2α and p-ERK (Fig. 4A-B). Depletion of KSR1 in these cells caused CK2α to become almost exclusively nuclear, while p-ERK levels were decreased dramatically. Human A375 melanoma cells, which carry a homozygous *BRAF*^{V600E} mutation, likewise displayed

intense perinuclear staining for p-ERK, CK2α and KSR1 (Fig. 4C). Moreover, the $BRAF^{V600E}$ oncoprotein itself was present in the nuclear-proximal region in A375 cells and its depletion greatly decreased p-ERK levels and disrupted the perinuclear trafficking of CK2α and KSR1.

Our results show that perinuclear signaling complexes (PSCs) containing p-ERK, CK2α and KSR1 are present in *HRAS*-, *KRAS*- and *BRAF*-transformed cells and occur independently of serum growth factors. These observations suggested that PSCs might be a common feature of cancer cells transformed by *RAS* or *BRAF* oncogenes. Accordingly, MDA-MD-231 cells (breast cancer; $KRAS^{G13D}$;$BRAF^{G464V}$), RKO cells (colorectal tumor; $BRAF^{V600E}$) and HepG2 cells (hepatocarcinoma; $NRAS^{Q61L}$) showed perinuclear localization of CK2α, p-ERK and KSR1 (Supplementary Fig. S3). Interestingly, HeLa cells (cervical carcinoma), which are not known to carry an activated RAS pathway oncogene, also displayed PSCs. Thus, PSCs are a feature of all tumor cells that we have analyzed, irrespective of their mutational landscape or driving oncogene, suggesting they may play a key role in establishing the neoplastic phenotype.

Since the PSCs are induced by oncogenic RAS or BRAF, we asked whether their formation requires the activity of RAS effector kinases. Treatment of $NIH3T3^{RAS}$ cells with the MEK1/2 inhibitor, U0126, strongly reduced p-ERK levels, as expected (Supplementary Fig. S4A). The drug also disrupted perinuclear localization of CK2α and KSR1, producing a pattern resembling that of non-transformed NIH3T3 cells; i.e., CK2α became more nuclear while KSR1 showed a pan-cytoplasmic distribution. Moreover, while TBB did not noticeably affect p-ERK levels as determined by IF staining, it produced a marked dispersal of p-ERK, CK2α and KSR1 from the perinuclear compartment. Both inhibitors also severely disrupted PSC formation in A549 cells (Fig. 4D) and A375 cells (Supplementary Fig. S4B). Similar effects were observed in A549 cells treated with the ERK1/2 inhibitor, SCH772984 (35) (Supplementary Fig. S4C), indicating that MEK-ERK signaling is critical for PSC formation.

To determine if disruption of PSCs by the MEK and CK2 inhibitors involves changes in KSR1 associations with p-ERK and CK2, we performed co-immunoprecipitation assays. Pyo-tagged KSR1 (36) was expressed in 293T cells, without or with $HRAS^{G12V}$, and pyo immunoprecipitates analyzed by IB. As shown in Fig. 4E, KSR1-CK2α binding was detectable in the absence of oncogenic RAS and this interaction was modestly increased in cells expressing $HRAS^{G12V}$. p-ERK also could be detected in the KSR1 complex when $HRAS^{G12V}$ was expressed. Treatment with U0126 blocked ERK activation, as expected, but did not appreciably affect CK2α binding to KSR1. Conversely, TBB did not reduce levels of p-ERK or its interaction with KSR1, but reversed the RAS-induced increase in KSR1-CK2α binding. We also observed an association between KSR1 and BRAF, and this interaction was not altered by either inhibitor. Together with the localization data, these results indicate that RAS-induced perinuclear translocation of p-ERK and CK2, while dependent on KSR1, does not involve major alterations in their physical association with the signaling scaffold. Instead, it appears that translocation of pre-existing complexes to the nuclear-proximal region is driven by oncogenic RAS and requires MEK-ERK and CK2 activity.

HRAS^{G12V}-C/EBPβ signaling and PSC formation requires endosomal trafficking

The perinuclear staining of p-ERK, CK2α and KSR1 was often punctate, indicating that these proteins might be associated with endosomal vesicles. This possibility is supported by the known role of endocytosis in growth factor receptor signaling (37) and studies showing that RAS pathway kinases can actively signal from endosomes and other internal membranes (38). Therefore, we asked whether C/EBPβ activation was sensitive to dynasore, a dynamin inhibitor that prevents coated vesicle formation and thus disrupts endocytosis (39). Dynasore blocked HRAS^{G12V}-induced activation of C/EBPβ$^{\Delta UTR}$ DNA binding in 293T cells and decreased phosphorylation on C/EBPβ Ser222 (Fig. 5A, left panel). Dynasore also reduced ERK-mediated phosphorylation on C/EBPβ Thr188 (Fig. 5A, right panel). However, the total levels of p-ERK induced by HRAS^{G12V} were unaffected by the inhibitor (right panel). These results suggest that access of p-ERK to its downstream target, C/EBPβ, but not ERK activation *per se* requires endocytic trafficking. In accordance with these results, dynasore also caused a significant decrease in RAS-induced activation of C/EBPβ-dependent SASP genes in MEFs (Supplementary Fig. S5A). Collectively, these data indicate that blocking endocytosis disconnects C/EBPβ from RAS signaling without affecting RAS-ERK pathway output.

The above findings imply that inhibiting endocytosis may affect RAS-induced perinuclear localization of p-ERK, CK2α and KSR1. Consistent with this prediction, perinuclear sorting of all three proteins in NIH3T3^{RAS} cells was abrogated by dynasore (Fig. 5B). Thus, endocytic trafficking plays a critical role in the subcellular compartmentalization of RAS pathway proteins and activation of C/EBPβ by oncogenic RAS.

CK2α and KSR1, but not p-ERK, localize to Rab11$^{(+)}$ perinuclear endosomes

We next investigated whether PSCs are associated with specific classes of endosomal vesicles. Members of the Rab family of small GTPases are endosomal proteins that regulate vesicle maturation and can be used as markers to identify specific classes of endocytic vesicles (40). Rab5 and Rab7/9 are associated with early and late endosomes, respectively. We did not detect co-localization of Rab5 or Rab7 with either p-ERK or CK2α in NIH3T3^{RAS} cells. However, Rab11, which is present on perinuclear recycling endosomes (41), displayed prominent co-localization with CK2α in A549 cells and partially overlapped with KSR1 (Fig. 5C). By contrast, p-ERK staining did not coincide with Rab11, suggesting that CK2 and p-ERK reside on different types of perinuclear endosomes. The same co-localization patterns were also seen in NIH3T3^{RAS} cells (Fig. 5D). The fact that CK2 and p-ERK associate with different endosomes was unexpected, as ERK, CK2α and KSR1 are predicted to be part of a common signaling complex, at least in GF-stimulated cells (31).

To test whether the co-localization of Rab11 with CK2α and KSR1 is dependent on endocytosis, we inhibited endocytosis prior to IF staining. Dynasore disrupted Rab11-CK2α and Rab11-KSR1 co-localization in both A549 cells (Fig. 5E) and NIH3T3^{RAS} cells (Fig. 5F). However, as was observed for the MEK and CK2 inhibitors, the drug did not appreciably affect KSR1 complex formation with CK2α, p-ERK or BRAF as determined by co-IP assays in 293T cells, although there was a modest reduction in the KSR1:p-ERK

interaction (Supplementary Fig. S5B). Thus, the dispersal of PSCs caused by endocytosis inhibitors is apparently not due to disruption of KSR1 signaling complexes.

Kras and *Braf*^{V600E}-driven mouse lung tumors display PSCs containing p-ERK, CK2α, KSR1, and BRAF

To extend our findings to an *in vivo* setting, we analyzed tumors from a *Kras*^{G12D}-driven mouse model of non-small-cell lung cancer (*Kras*^{LA2}) (22). These mice spontaneously develop mainly lung tumors which progress to adenocarcinomas (ADCs) (Fig. 6A). We performed IF staining for RAS pathway proteins on tumor-bearing lung sections and adjacent normal tissue (Fig. 6B). As expected, normal lung tissue showed much lower levels of p-ERK compared to the tumor area. CK2α and KSR1 were also significantly up-regulated in the ADCs, consistent with observations that expression of these two proteins can be increased in cancers (42,43). Notably, the tumor cells displayed clearly visible perinuclear rings containing p-ERK, CK2α, KSR1 and BRAF. Although expressed at lower levels, CK2α and KSR1 exhibited diffuse cytoplasmic staining in normal lung epithelium, in marked contrast to their definitive perinuclear localization in ADC cells. While BRAF levels were similar between normal and tumor cells, the protein showed a distinct perinuclear distribution in ADCs.

We also analyzed lung tumors from mice carrying a conditional *Braf*^{V600E} allele which, upon activation by Cre recombinase (instillation of Ad.Cre virus), develop mainly benign adenomas with certain features of senescence (23) (Fig. 6A). Immunostaining showed that these differentiated tumors displayed distinct perinuclear staining for KSR1, CK2α and BRAF as compared to normal tissue (Fig. 6C). Activated ERK was increased in tumors but not to the levels seen in *Kras* tumors. Nonetheless, cells with perinuclear p-ERK staining could be observed. Due to the rapid development of terminal disease caused by high adenoma burdens, we were unable to analyze progression to ADCs in this model. However, PSCs are clearly present even in these early stage adenomas, consistent with their induction by RAS pathway activation.

PSCs are induced transiently in serum-stimulated normal cells with delayed kinetics corresponding to C/EBPβ phosphorylation and activation of DNA binding

Since PSCs are observed in tumor cells with dysregulated RAS signaling, we sought to determine if these structures are also induced in normal cells through activation of the RAS pathway by growth factors. We first analyzed the kinetics of C/EBPβ activation by serum GFs in NIH3T3 cells, since this protein is a physiological target of the RAS pathway. Because endogenous C/EBPβ in these cells is not appreciably activated by RAS signaling due to 3′UTR inhibition, we transfected the cells with a C/EBPβ$^{\Delta UTR}$ construct. The cells were then serum starved, re-stimulated and nuclear extracts prepared over a time course and analyzed for C/EBPβ DNA binding and phosphorylation (Fig. 7A, left panel). The low basal C/EBPβ DNA binding in resting cells remained suppressed at 2 hr but was activated at 4 and 6 hr, and subsequently returned to baseline levels by 12 hr. Analysis of C/EBPβ phosphorylation showed an increase in p-Ser222 levels at 4 and 6 hr, coinciding with elevated DNA binding. p-Thr188 was also induced but did not appear until 6 hr, and phosphorylation on both sites declined at 12 hr. These results are consistent with our

findings that Ser222 is critical for activation of DNA binding (Fig. 1B), whereas Thr188 is dispensable (18). By contrast, C/EBPβ expressed from the C/EBPβ^{UTR} construct was refractory to serum-induced activation at all time points (Fig. 7A, right panel). In primary MEFs, where UPA is diminished (20), endogenous C/EBPβ DNA binding was also transiently increased at 4 hr post-stimulation (Supplementary Fig. S6A). Thus, delayed kinetics of GF-induced C/EBPβ activation are observed in both systems.

To further understand the timing and KSR1 dependence of GF-induced signaling and the relationship to C/EBPβ activation, we performed IF imaging of RAS pathway proteins over an 8-hour time course in NIH3T3 cells (Fig. 7B). CK2α, p-ERK, KSR1 and BRAF each displayed dynamic, GF-induced localization to the perinuclear region, albeit with slightly differing kinetics. Strikingly, CK2α was mostly nuclear in unstimulated cells, became diffusely cytoplasmic at 2 hr, tightly perinuclear at 4 and 6 hr, and returned to nuclear distribution by 8 hr. Thus, the perinuclear appearance of CK2α coincides closely with phosphorylation on C/EBPβ Ser222. This relationship with C/EBPβ modification was also observed for p-ERK, which became distinctly perinuclear only at 6 hr, mirroring the kinetics of phosphorylation on its cognate C/EBPβ site, Thr188. KSR1 also underwent perinuclear translocation beginning at 4 hr and continuing through 6 hr. BRAF was partially nuclear in resting cells, but became more diffusely cytoplasmic at 2 hr and exhibited a more definitive perinuclear ring at 4 and 6 hr. Similar GF-induced PSC formation was observed in a non-transformed human mammary epithelial cell line, MCF10A (Supplementary Fig. S6B). Although the overall kinetics were more rapid than in NIH3T3 cells, perinuclear localization of CK2α again slightly preceded that of p-ERK, and KSR1 and BRAF trafficking was similar to CK2α. These findings indicate that delayed PSC formation is a general feature of physiological GF-induced signaling.

C/EBPβ phosphorylation by ERK in NIH3T3 cells was dependent on KSR1, as p-T188 levels analyzed by immunoblotting at 6 hr post-stimulation were reduced more than 3-fold in KSR1-depleted cells compared to controls (Fig. 7C). Notably, p-ERK levels were increased in siRNA control cells at 6 hr compared to 0 hr, but also were only modestly reduced in siKSR1-transfected cells relative to control cells, indicating that impaired phosphorylation on C/EBPβ Thr188 in KSR1-depleted cells is separable from ERK activity *per se*. Accordingly, GF-induced formation of p-ERK PSCs at 6 hr was disrupted in KSR1-depleted cells, as p-ERK was present but remained broadly distributed in the cytoplasm (Supplementary Fig. S7A). Similarly, perinuclear translocation of CK2α at 4-6 hr was abrogated by KSR1 knockdown. These findings, together with the results from tumor cells, demonstrate a critical role for KSR1 in PSC formation by mutant or physiological RAS signaling.

Our data indicate that C/EBPβ is phosphorylated by ERK exclusively in the perinuclear cytoplasm in a KSR1-dependent manner. However, other transcription factors that are targets of GF-activated ERK kinase, particularly those of the ETS family such as Elk-1, are phosphorylated in the nucleus (44,45). Therefore, we asked whether KSR1 depletion affects GF-induced phosphorylation on the Elk-1 ERK site (Ser383). As shown in Supplementary Fig. S7B, p-Ser383 was detected 10 minutes after serum treatment and was maintained through 1 hr, declining thereafter to nearly baseline levels by 4 hr. However, this

modification was completely unaffected by KSR1 depletion. Moreover, neither nuclear nor cytoplasmic p-ERK levels were decreased in serum-stimulated cells depleted of KSR1. These results indicate that phosphorylation of Elk-1 on Ser383 does not involve p-ERK localized to PSCs, consistent with the impaired activation of Elk-1 that has been observed in senescent cells, which display cytoplasmic p-ERK (45) (also see Fig. 3E). Thus, ERK-mediated phosphorylation of C/EBPβ and Elk-1 shows differential kinetics, subcellular locations, and dependence on KSR1.

Discussion

Here, we have identified and characterized perinuclear signaling complexes and demonstrate their importance in mutant and physiological RAS signaling. “PSCs” refers to the perinuclear localization of several RAS pathway proteins, including activated ERK, CK2, KSR1, and BRAF. In addition to their subcellular location, PSCs are defined by 1) their persistence in tumor cells deprived of growth factors, 2) their induction by driver oncogenes such as $KRAS^{G12D}$ and $BRAF^{V600E}$, 3) their dependence on the signaling scaffold, KSR1, 4) the requirement for MEK-ERK and CK2 activity, and 5) their dependence on endocytosis and association with perinuclear endosomes. PSCs are characteristic features of tumor cells and are not present in non-transformed, serum-deprived cells, but can be transiently induced by serum GFs with delayed kinetics (2-6 hr post-stimulation). The latter finding defines a late phase of GF signaling that is distinct from early events such as ERK activation and its translocation to the nucleus, which occur within minutes of GF receptor engagement (46). The striking spatial similarities between GF-induced PSCs present at 4-6 hr and those in tumor cells suggest that dysregulated RAS pathway signaling persistently activates the delayed phase of GF signaling to drive oncogenesis.

PSCs in tumor cells as well as those induced by GFs are highly dependent on KSR1. Moreover, PSC formation correlates with KSR1 recruitment to the perinuclear region upon RAS pathway activation. Depletion of KSR1 in tumor cells severely curtailed ERK activation, as expected, but also affected p-ERK localization. Conversely, KSR1 ablation in serum-starved, non-transformed cells modestly increased basal p-ERK levels and its absence did not impair GF-induced activation of ERK, its ability to enter the nucleus or activation of a known nuclear target, Elk-1. Thus, tumor cells exhibit much greater dependence on KSR1 than normal cells, which may explain why $KSR1^{-/-}$ mice are viable but display resistance to RAS-induced tumorigenesis (21,47).

The perinuclear compartmentalization of RAS effector kinases plays a key role in regulating transmission of RAS signals to C/EBPβ. In tumor cells, PSC-associated kinases are physically distinct from a peripheral cytoplasmic region where *Cebpb* transcripts are localized by 3′UTR-mediated mRNA trafficking (20). This partitioning suppresses RAS-driven activation of C/EBPβ by preventing ERK and CK2 kinases from accessing C/EBPβ, which is translated from mRNAs restricted to the cell periphery (Fig. 2). By maintaining C/EBPβ and perhaps other anti-oncogenic proteins in a low activity state, the UPA mechanism contributes to senescence bypass in tumor cells. PSCs are also induced by mutant RAS in primary MEFs undergoing OIS. However, UPA is suppressed in these cells, allowing endogenous C/EBPβ to become activated. When C/EBPβ is expressed without its 3′UTR in

tumor cells or when UPA is absent, as in MEFs, its activation can still be blocked by disruption of PSCs (e.g., by mutation/depletion of KSR1 or inhibition of endocytosis). Thus, PSCs anchored to perinuclear endosomes provide an essential signaling platform for C/EBPβ phosphorylation/activation by RAS effector kinases in senescent cells. As PSCs occur in both transformed and senescent cells, the UPA status (on or off) determines whether C/EBPβ is activated to promote senescence or is maintained in a low activity state to facilitate tumor growth (Supplementary Fig. S7C).

Our results indicate that CK2 functions as a RAS effector kinase, as its ability to phosphorylate C/EBPβ is greatly increased by oncogenic or physiological RAS signaling (Fig. 2A and Fig. 7A). Since the intrinsic kinase activity of CK2 is constitutive (48), we propose that the RAS-induced functionality of CK2 involves its re-localization to perinuclear endosomes, where it can access substrates such as C/EBPβ. CK2α and p-ERK become predominantly perinuclear at 4 and 6 hr, respectively, following GF stimulation. The timing of their re-localization corresponds to phosphorylation on the C/EBPβ CK2 and ERK sites (Ser222 and Thr188) (Fig. 7). These results provide compelling evidence that modification of C/EBPβ by CK2 and p-ERK occurs exclusively in the perinuclear compartment. The kinetic data also support our observation that the two kinases reside on different types of endosomal vesicles. It is tempting to speculate that the differential timing of C/EBPβ phosphorylation by CK2 and ERK involves maturation of $Rab11^{(+)}$, CK2-containing endosomes into $Rab11^{(-)}$ vesicles harboring p-ERK, possibly with C/EBPβ remaining associated and undergoing serial phosphorylation by the two kinases. Clearly, further studies are needed to fully characterize the different classes of PSC-associated endosomes, the relationships between them, and how such compartmentalization controls the activation of substrates such as C/EBPβ.

We observed that activated ERK in tumor cells is predominantly perinuclear and very little p-ERK is detected in the nucleus. This finding stands in contrast to the common assumption that ERK-regulated transcription factors such as c-Myc and c-Fos − important drivers of cell proliferation and cancer − are phosphorylated by ERK in the nucleus (49). Although we cannot rule out the possibility that a small fraction of nuclear ERK performs these functions, our data strongly indicate that many TF substrates in tumor cells are phosphorylated by active ERK in the perinuclear cytoplasm. Several scaffold proteins have been described that tether ERK to cytoplasmic locations and endosomes, including p18, a lipid raft adaptor (50), and the p14-MP1 complex (51,52). It will be important to determine the involvement of these and other cytoplasmic anchoring proteins in GF-induced and tumor-associated PSCs. GFs that signal through G protein-coupled receptors (GPCRs) are known to induce sustained, cytoplasmic localization of p-ERK though association with the signaling scaffold, β-arrestin, on endosomes (53,54). However, the function and targets of this cytoplasmic pool of activate ERK are largely unknown. By analogy to C/EBPβ, it is possible that the perinuclear p-ERK induced by GPCR signaling is also used to establish substrate accessibility, perhaps involving UPA-like mRNA localization mechanisms. This could be a common strategy to control signal transmission to downstream targets and govern biological responses to extracellular cues.

All tumor cells we have examined to date display the two essential features of UPA − PSCs and peripheral localization of *Cebpb* transcripts − even when they lack known RAS pathway mutations. Therefore, PSCs appear to be key hallmarks of cancer cells. The spatial reorganization of effector kinases in tumor cells may drive neoplastic growth and tumorigenesis, with PSCs directing the modification of critical oncogenic substrates at perinuclear sites. The presence of PSCs across a wide range of tumors suggests their formation can be induced by a variety of driver mutations, not just those affecting core RAS pathway components. Thus, future characterizations of rare or non-canonical tumor-associated mutations should include determining whether the mutant proteins promote PSC formation and/or are components of these signaling complexes. In addition, PSCs could potentially be used as biomarkers for cancer detection and assessing therapeutic responses.

Supplementary Material

Refer to Web version on PubMed Central for supplementary material.

Acknowledgments

We thank members of the NCI-Frederick Optical Microscopy and Analysis Laboratory for confocal microscopy support, Karen Saylor and Nancy Martin for animal husbandry and genotyping, and Allen Kane (Scientific Publications, Graphics & Media, Leidos Biomedical Research, Inc., Frederick National Laboratory for Cancer Research) for preparation of figures. This research was supported by the Intramural Research Program of the NIH, National Cancer Institute, Center for Cancer Research. The content of this publication does not necessarily reflect the views or policies of the Department of Health and Human Services, nor does mention of trade names, commercial products, or organizations imply endorsement by the U.S. Government.

References

1. Malumbres M, Barbacid M. RAS oncogenes: the first 30 years. Nat Rev Cancer. 2003; 3:459–65. [PubMed: 12778136]
2. Hanahan D, Weinberg RA. Hallmarks of cancer: the next generation. Cell. 2011; 144:646–74. [PubMed: 21376230]
3. McKay MM, Morrison DK. Integrating signals from RTKs to ERK/MAPK. Oncogene. 2007; 26:3113–21. [PubMed: 17496910]
4. Network TCGAR. Comprehensive molecular profiling of lung adenocarcinoma. Nature. 2014; 511:543–50. [PubMed: 25079552]
5. Yip-Schneider MT, Lin A, Barnard D, Sweeney CJ, Marshall MS. Lack of elevated MAP kinase (Erk) activity in pancreatic carcinomas despite oncogenic K-ras expression. Int J Oncol. 1999; 15:271–9. [PubMed: 10402237]
6. Serrano M, Lin AW, McCurrach ME, Beach D, Lowe SW. Oncogenic ras provokes premature cell senescence associated with accumulation of p53 and p16INK4a. Cell. 1997; 88:593–602. [PubMed: 9054499]
7. Campisi J. Senescent cells, tumor suppression, and organismal aging: good citizens, bad neighbors. Cell. 2005; 120:513–22. [PubMed: 15734683]
8. Collado M, Blasco MA, Serrano M. Cellular senescence in cancer and aging. Cell. 2007; 130:223–33. [PubMed: 17662938]
9. Huggins CJ, Malik R, Lee S, Salotti J, Thomas S, Martin N, et al. C/EBPgamma suppresses senescence and inflammatory gene expression by heterodimerizing with C/EBPbeta. Mol Cell Biol. 2013; 33:3242–58. [PubMed: 23775115]
10. Kuilman T, Michaloglou C, Vredeveld LC, Douma S, van Doorn R, Desmet CJ, et al. Oncogene-induced senescence relayed by an interleukin-dependent inflammatory network. Cell. 2008; 133:1019–31. [PubMed: 18555778]

11. Sebastian T, Malik R, Thomas S, Sage J, Johnson PF. C/EBPbeta cooperates with RB:E2F to implement Ras(V12)-induced cellular senescence. EMBO J. 2005; 24:3301–12. [PubMed: 16107878]
12. Acosta JC, O'Loghlen A, Banito A, Guijarro MV, Augert A, Raguz S, et al. Chemokine signaling via the CXCR2 receptor reinforces senescence. Cell. 2008; 133:1006–18. [PubMed: 18555777]
13. Freund A, Orjalo AV, Desprez PY, Campisi J. Inflammatory networks during cellular senescence: causes and consequences. Trends Mol Med. 2010; 16:238–46. [PubMed: 20444648]
14. Kuilman T, Michaloglou C, Mooi WJ, Peeper DS. The essence of senescence. Genes Dev. 2010; 24:2463–79. [PubMed: 21078816]
15. Kowenz-Leutz E, Twamley G, Ansieau S, Leutz A. Novel mechanism of C/EBP●β (NF-M) transcriptional control: activation through derepression. Genes Dev. 1994; 8:2781–91. [PubMed: 7958933]
16. Williams SC, Baer M, Dillner AJ, Johnson PF. CRP2 (C/EBPβ)●contains a bipartite regulatory domain that controls transcriptional activation, DNA binding and cell specificity. EMBO J. 1995; 14:3170–83. [PubMed: 7621830]
17. Lee S, Miller M, Shuman JD, Johnson PF. CCAAT/Enhancer-binding protein beta DNA binding is auto-inhibited by multiple elements that also mediate association with p300/CREB-binding protein (CBP). J Biol Chem. 2010; 285:21399–410. [PubMed: 20452968]
18. Lee S, Shuman JD, Guszczynski T, Sakchaisri K, Sebastian T, Copeland TD, et al. RSK-mediated phosphorylation in the C/EBP{beta} leucine zipper regulates DNA binding, dimerization, and growth arrest activity. Mol Cell Biol. 2010; 30:2621–35. [PubMed: 20351173]
19. Nakajima T, Kinoshita S, Sasagawa T, Sasaki K, Naruto M, Kishimoto T, et al. Phosphorylation at threonine-235 by a ras-dependent mitogen-activated protein kinase cascade is essential for transcription factor NF-IL6. Proc Natl Acad Sci USA. 1993; 90:2207–11. [PubMed: 8384717]
20. Basu SK, Malik R, Huggins CJ, Lee S, Sebastian T, Sakchaisri K, et al. 3′UTR elements inhibit Ras-induced C/EBPbeta post-translational activation and senescence in tumour cells. EMBO J. 2011; 30:3714–28. [PubMed: 21804532]
21. Nguyen A, Burack WR, Stock JL, Kortum R, Chaika OV, Afkarian M, et al. Kinase suppressor of Ras (KSR) is a scaffold which facilitates mitogen-activated protein kinase activation in vivo. Mol Cell Biol. 2002; 22:3035–45. [PubMed: 11940661]
22. Johnson L, Mercer K, Greenbaum D, Bronson RT, Crowley D, Tuveson DA, et al. Somatic activation of the K-ras oncogene causes early onset lung cancer in mice. Nature. 2001; 410:1111–6. [PubMed: 11323676]
23. Dankort D, Filenova E, Collado M, Serrano M, Jones K, McMahon M. A new mouse model to explore the initiation, progression, and therapy of BRAFV600E-induced lung tumors. Genes Dev. 2007; 21:379–84. [PubMed: 17299132]
24. McKay MM, Ritt DA, Morrison DK. RAF inhibitor-induced KSR1/B-RAF binding and its effects on ERK cascade signaling. Curr Biol. 2011; 21:563–8. [PubMed: 21458265]
25. Parkin SE, Baer M, Copeland TD, Schwartz RC, Johnson PF. Regulation of CCAAT/enhancer-binding protein (C/EBP) activator proteins by heterodimerization with C/EBPgamma (Ig/EBP). J Biol Chem. 2002; 277:23563–72. [PubMed: 11980905]
26. Rook MS, Lu M, Kosik KS. CaMKIIalpha 3′ untranslated region-directed mRNA translocation in living neurons: visualization by GFP linkage. J Neurosci. 2000; 20:6385–93. [PubMed: 10964944]
27. Scheffler JM, Schiefermeier N, Huber LA. Mild fixation and permeabilization protocol for preserving structures of endosomes, focal adhesions, and actin filaments during immunofluorescence analysis. Methods Enzymol. 2014; 535:93–102. [PubMed: 24377919]
28. Whelan DR, Bell TD. Image artifacts in single molecule localization microscopy: why optimization of sample preparation protocols matters. Scientific reports. 2015; 5:7924. [PubMed: 25603780]
29. Olsten ME, Litchfield DW. Order or chaos? An evaluation of the regulation of protein kinase CK2. Biochemistry and cell biology = Biochimie et biologie cellulaire. 2004; 82:681–93. [PubMed: 15674436]
30. Siddiqui-Jain A, Drygin D, Streiner N, Chua P, Pierre F, O'Brien SE, et al. CX-4945, an orally bioavailable selective inhibitor of protein kinase CK2, inhibits prosurvival and angiogenic

signaling and exhibits antitumor efficacy. Cancer Research. 2010; 70:10288–98. [PubMed: 21159648]

31. Ritt DA, Zhou M, Conrads TP, Veenstra TD, Copeland TD, Morrison DK. CK2 Is a component of the KSR1 scaffold complex that contributes to Raf kinase activation. Curr Biol. 2007; 17:179–84. [PubMed: 17174095]
32. Kortum RL, Johnson HJ, Costanzo DL, Volle DJ, Razidlo GL, Fusello AM, et al. The molecular scaffold kinase suppressor of Ras 1 is a modifier of RasV12-induced and replicative senescence. Mol Cell Biol. 2006; 26:2202–14. [PubMed: 16507997]
33. Kortum RL, Lewis RE. The molecular scaffold KSR1 regulates the proliferative and oncogenic potential of cells. Mol Cell Biol. 2004; 24:4407–16. [PubMed: 15121859]
34. McKay MM, Ritt DA, Morrison DK. Signaling dynamics of the KSR1 scaffold complex. Proc Natl Acad Sci USA. 2009; 106:11022–7. [PubMed: 19541618]
35. Morris EJ, Jha S, Restaino CR, Dayananth P, Zhu H, Cooper A, et al. Discovery of a novel ERK inhibitor with activity in models of acquired resistance to BRAF and MEK inhibitors. Cancer Discov. 2013; 3:742–50. [PubMed: 23614898]
36. Cacace AM, Michaud NR, Therrien M, Mathes K, Copeland T, Rubin GM, et al. Identification of constitutive and ras-inducible phosphorylation sites of KSR: implications for 14-3-3 binding, mitogen-activated protein kinase binding, and KSR overexpression. Mol Cell Biol. 1999; 19:229–40. [PubMed: 9858547]
37. Mor A, Philips MR. Compartmentalized Ras/MAPK signaling. Annu Rev Immunol. 2006; 24:771–800. [PubMed: 16551266]
38. Fehrenbacher N, Bar-Sagi D, Philips M. Ras/MAPK signaling from endomembranes. Mol Oncol. 2009; 3:297–307. [PubMed: 19615955]
39. Macia E, Ehrlich M, Massol R, Boucrot E, Brunner C, Kirchhausen T. Dynasore, a cell-permeable inhibitor of dynamin. Dev Cell. 2006; 10:839–50. [PubMed: 16740485]
40. Scita G, Di Fiore PP. The endocytic matrix. Nature. 2010; 463:464–73. [PubMed: 20110990]
41. Schlierf B, Fey GH, Hauber J, Hocke GM, Rosorius O. Rab11b is essential for recycling of transferrin to the plasma membrane. Exp Cell Res. 2000; 259:257–65. [PubMed: 10942597]
42. Wang L, Jiang CF, Li DM, Ge X, Shi ZM, Li CY, et al. MicroRNA-497 inhibits tumor growth and increases chemosensitivity to 5-fluorouracil treatment by targeting KSR1. Oncotarget. 2016; 7:2660–71. [PubMed: 26673620]
43. Chua MM, Ortega CE, Sheikh A, Lee M, Abdul-Rassoul H, Hartshorn KL, et al. CK2 in Cancer: Cellular and Biochemical Mechanisms and Potential Therapeutic Target. Pharmaceuticals. 2017; 10
44. Sharrocks AD. The ETS-domain transcription factor family. Nat Rev Mol Cell Biol. 2001; 2:827–37. [PubMed: 11715049]
45. Tresini M, Lorenzini A, Frisoni L, Allen RG, Cristofalo VJ. Lack of Elk-1 phosphorylation and dysregulation of the extracellular regulated kinase signaling pathway in senescent human fibroblast. Exp Cell Res. 2001; 269:287–300. [PubMed: 11570821]
46. Murphy LO, Blenis J. MAPK signal specificity: the right place at the right time. Trends Biochem Sci. 2006; 31:268–75. [PubMed: 16603362]
47. Lozano J, Xing R, Cai Z, Jensen HL, Trempus C, Mark W, et al. Deficiency of kinase suppressor of Ras1 prevents oncogenic ras signaling in mice. Cancer Research. 2003; 63:4232–8. [PubMed: 12874031]
48. Olsen BB, Guerra B, Niefind K, Issinger OG. Structural basis of the constitutive activity of protein kinase CK2. Methods Enzymol. 2010; 484:515–29. [PubMed: 21036248]
49. Mebratu Y, Tesfaigzi Y. How ERK1/2 activation controls cell proliferation and cell death: Is subcellular localization the answer? Cell Cycle. 2009; 8:1168–75. [PubMed: 19282669]
50. Nada S, Hondo A, Kasai A, Koike M, Saito K, Uchiyama Y, et al. The novel lipid raft adaptor p18 controls endosome dynamics by anchoring the MEK-ERK pathway to late endosomes. EMBO J. 2009; 28:477–89. [PubMed: 19177150]
51. Teis D, Taub N, Kurzbauer R, Hilber D, de Araujo ME, Erlacher M, et al. p14-MP1-MEK1 signaling regulates endosomal traffic and cellular proliferation during tissue homeostasis. J Cell Biol. 2006; 175:861–8. [PubMed: 17178906]

52. Teis D, Wunderlich W, Huber LA. Localization of the MP1-MAPK scaffold complex to endosomes is mediated by p14 and required for signal transduction. Dev Cell. 2002; 3:803–14. [PubMed: 12479806]

53. Caunt CJ, Finch AR, Sedgley KR, McArdle CA. Seven-transmembrane receptor signalling and ERK compartmentalization. Trends Endocrinol Metab. 2006; 17:276–83. [PubMed: 16890451]

54. Lefkowitz RJ, Rajagopal K, Whalen EJ. New roles for beta-arrestins in cell signaling: not just for seven-transmembrane receptors. Mol Cell. 2006; 24:643–52. [PubMed: 17157248]

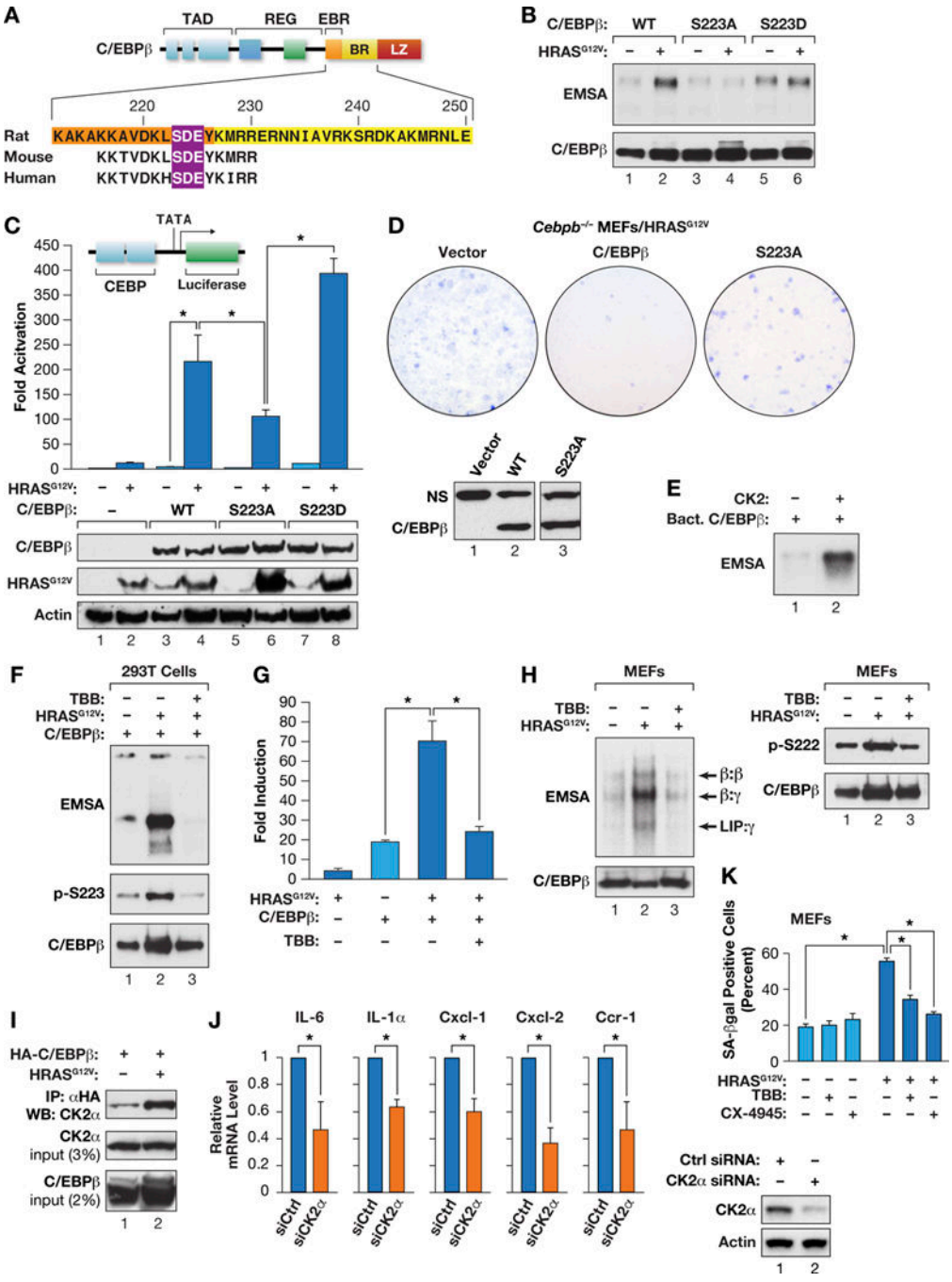

Figure 1.

Ser222/223 is a RAS-induced CK2 phosphoacceptor that regulates C/EBPβ DNA-binding and cytostatic activity. **A**, Diagram showing functional domains of C/EBPβ and the amino acid sequence of the bZIP region (rat). The putative CK2 site is boxed and its conservation in mouse and human homologs is depicted. TAD, transactivation domain; REG, regulatory region; EBR, extended basic region; BR, basic region; LZ, leucine zipper. **B**, EMSA assay showing the effect of Ser223 substitutions on RAS-induced C/EBPβ DNA-binding activity. WT and mutant rat C/EBPβ constructs (LAP isoform) lacking 3′UTR sequences were

expressed without or with an $HRAS^{G12V}$ vector in 293T cells. In this and all subsequent experiments involving oncogenic RAS, the cells were serum-starved for 16 hr prior to harvesting to prevent growth factor-induced RAS signaling. Nuclear extracts were prepared and analyzed by EMSA using a radiolabeled C/EBP binding site probe. C/EBPβ protein levels (bottom) were equalized among the various samples prior to EMSA. The EMSA image was cropped to include only the area containing protein-DNA complexes. **C**, Transactivation assays of WT and Ser223 mutant C/EBPβ proteins. 293T cells were transfected with the indicated C/EBPβ vectors, ± $HRAS^{G12V}$, and a 2X C/EBP-Luc reporter construct (inset). Luciferase activity of the reporter alone was normalized to 1; all other values represent fold activation relative to the control. n = 3; error bars represent SD. Bottom panel shows levels of overexpressed C/EBPβ and $HRAS^{G12V}$ proteins. **D**, Ser223 phosphorylation is required for the cytostatic activity of C/EBPβ in MEFs. $HRAS^{G12V}$-expressing *Cebpb*$^{-/-}$ MEFs, which bypass senescence and form colonies efficiently (11), were infected with retroviruses expressing WT or S223A C/EBPβ proteins or the empty vector, and colony formation was analyzed. Bottom panel shows C/EBPβ protein levels; NS (non-specific band, which serves as a loading control). **E**, *In vitro* phosphorylation of recombinant C/EBPβ by purified CK2 stimulates its DNA-binding activity. Equal quantities of purified C/EBPβ were incubated with either buffer or CK2 holoenzyme and ATP, and analyzed by EMSA. **F**, The CK2 inhibitor, 4,5,6,7-tetrabromo-2-azabenzimidazole (TBB), blocks $HRAS^{G12V}$-induced augmentation of C/EBPβ DNA binding and inhibits phosphorylation on Ser223. The EMSA was performed as described in panel **B**. In lane 3, 10 μM TBB was added to the cells 16 hr prior to harvest. Immunoblots for total C/EBPβ and p-S223 C/EBPβ levels are shown below. **G**, TBB inhibits C/EBPβ transcriptional activity. Transactivation assays were performed as described in panel **C**, with 10 μM TBB added to the cells as indicated. n = 3; error bars represent SD. **H**, CK2 activity is required for $HRAS^{G12V}$-induced C/EBPβ DNA binding in MEFs. Cells were infected with control or $HRAS^{G12V}$ retroviruses and treated with vehicle or 10 μM TBB for 16 hr. Nuclear extracts were analyzed by EMSA (left); the various complexes correspond to different dimeric forms of C/EBPβ, as indicated by arrows (9). Right panel shows C/EBPβ p-S222 levels in the lysates compared to total C/EBPβ. **I**, CK2 association with C/EBPβ is stimulated by oncogenic RAS signaling. HA-tagged C/EBPβ was expressed in 293T cells ± $HRAS^{G12V}$ and immunoprecipitated using an HA antibody. The bound fraction was probed for CK2α. **J**, CK2 is required for efficient C/EBPβ-induced expression of SASP genes in $NIH3T3^{RAS}$ cells. NIH3T3 cells expressing $HRAS^{G12V}$ and $C/EBP\beta^{\Delta UTR}$ were transfected with control or CK2α siRNAs and analyzed for expression of SASP genes by qRT-PCR. Expression of each gene in siCtrl cells was set to 1, and levels in CK2-depleted cells were calculated as a fraction of the control value. n = 3, each sample assayed in triplicate; error bars represent SD; *$p < 0.05$. Right panel: immunoblot showing CK2α levels in control and siRNA depleted cells. **K**, CK2 activity is essential for OIS. MEFs were infected with control or $HRAS^{G12V}$-expressing retroviruses and cells were immediately treated with vehicle, 10 μM TBB, or 5 μM CX-4945 (30) for the duration of the experiment. After 11 days, cells were stained for SA-βGal and the proportion of senescent cells was quantitated. 10 fields containing a total of 200-300 cells were analyzed for each cell population; error bars represent SD; *$p < 0.05$.

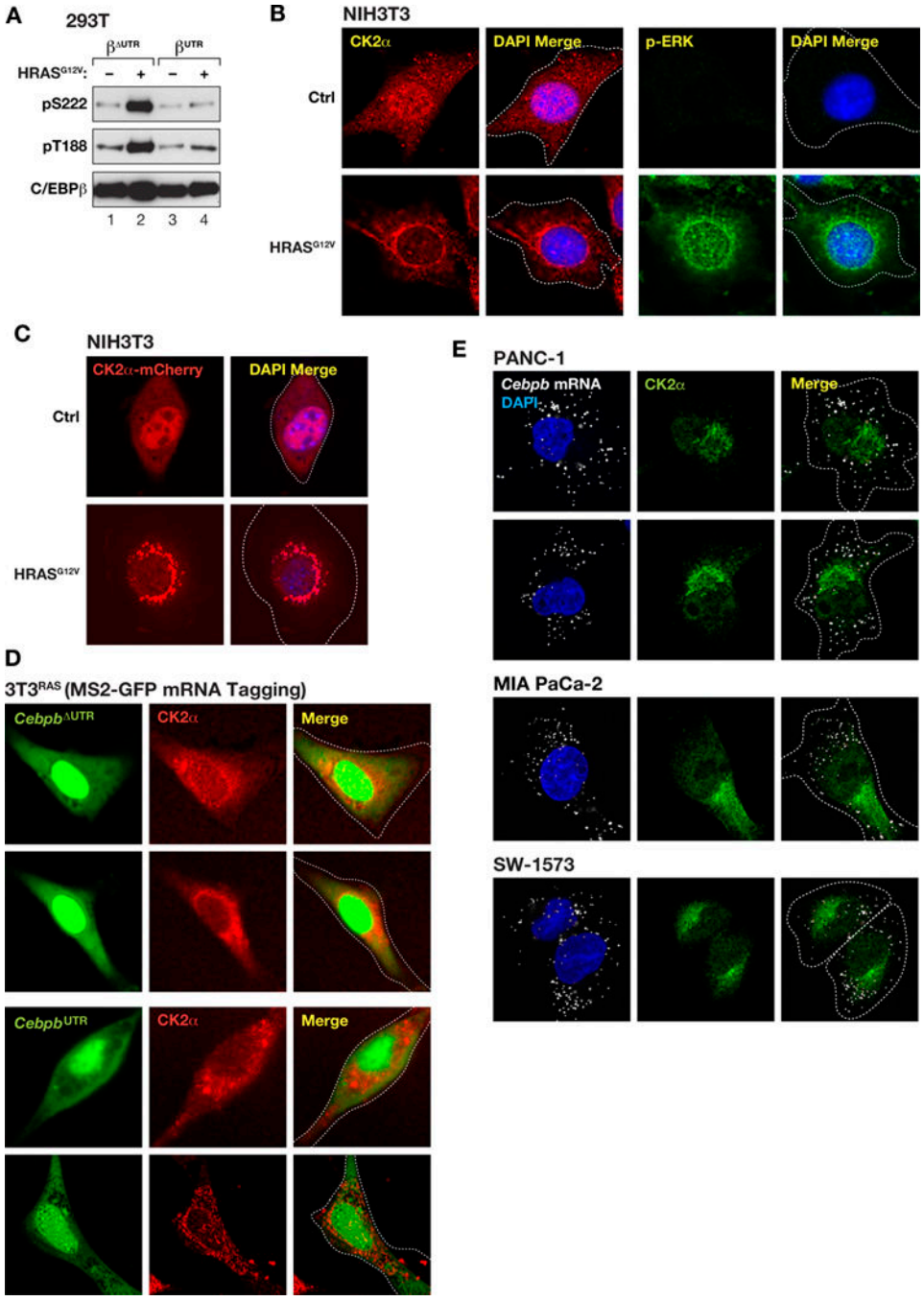

Figure 2.

RAS-induced phosphorylation on C/EBPβ Ser222 is inhibited by the *Cebpb* 3′UTR through mutually exclusive subcellular localization of *Cebpb* mRNA and CK2. **A**, The *Cebpb* 3′UTR suppresses $HRAS^{G12V}$-induced phosphorylation on Ser222 (CK2) and Thr188 (ERK). 293T cells were transfected with $Cebpb^{\Delta UTR}$ or $Cebpb^{UTR}$ constructs, ± $HRAS^{G12V}$, and nuclear extracts were analyzed by immunoblotting using the indicated phospho-specific and total C/EBPβ antibodies. **B**, $HRAS^{G12V}$ induces CK2α re-localization from the nucleus to a perinuclear cytoplasmic location. Confocal immunofluorescence

micrographs are shown for control and RAS-expressing cells immunostained for CK2α. The right panels show immunostaining for p-ERK in the same cell populations. **C**, Fluorescently-tagged CK2α expressed in NIH3T3 cells undergoes nuclear to perinuclear translocation in response to oncogenic HRAS. Images are from live cells stably expressing a CK2α-mCherry fusion construct. **D**, *Cebpb*^{UTR} transcripts are excluded from a perinuclear region that contains CK2α in 3T3^{RAS} cells. Confocal images show MS2-GFP-tethered *Cebpb* transcripts that contain or lack the 3′UTR (*Cebpb*^{UTR} and *Cebpb*$^{\Delta UTR}$, respectively) (20). The cells were also immunostained for CK2α. The free MS2-GFP-nls reporter (not bound to *Cebpb* transcripts) is responsible for the strong nuclear fluorescence. The mRNA-bound reporter is cytoplasmic. **E**, Endogenous *CEBPB* transcripts display peripheral localization that is largely non-overlapping with CK2α in human tumor cells. *CEBPB* mRNA was visualized in PANC-1 and MIA PaCa-2 pancreatic ductal adenocarcinoma cells and SW-1573 lung carcinoma cells using single molecule RNA fluorescence in situ hybridization (RNA FISH). The cells were also immunostained for CK2α. Examples of two cells are shown for PANC-1.

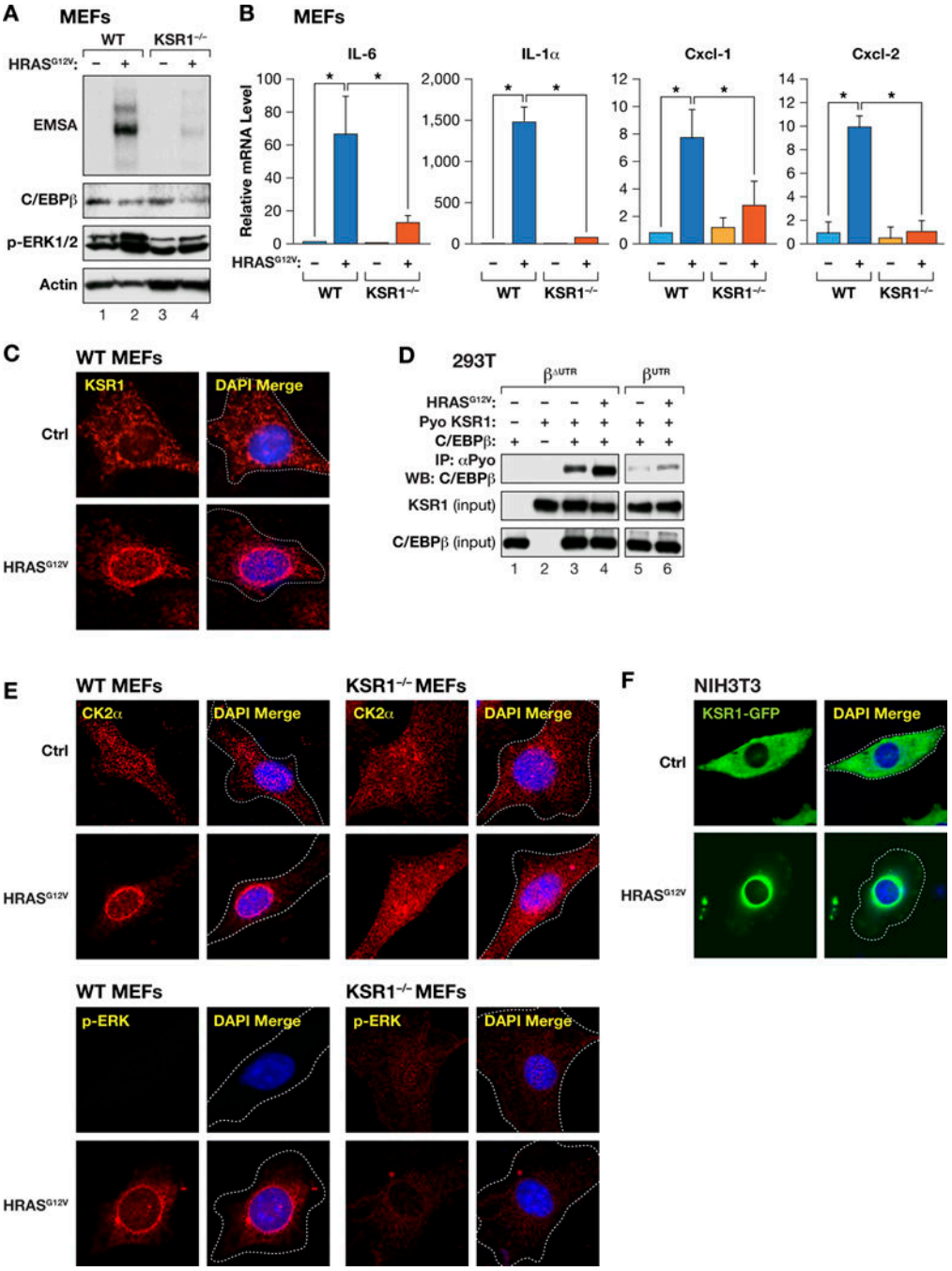

Figure 3.

KSR1 is required for C/EBPβ activation and expression of SASP genes in MEFs and undergoes perinuclear translocation in HRAS^{G12V}-expressing cells. **A**, Induction of C/EBPβ DNA binding by HRAS^{G12V} in MEFs is dependent on KSR1. *WT* and *KSR1*$^{-/-}$ MEFs were infected with control and HRAS^{G12V}-expressing retroviruses. Cell lysates were prepared and analyzed by EMSA using a C/EBP binding site probe. Levels of C/EBPβ and p-ERK1/2 in each lysate were analyzed by immunoblotting (bottom). **B**, KSR1 is essential for RAS-induced expression of SASP genes in senescent fibroblasts. Control and HRAS^{G12V}-

expressing *WT* and *KSR1*$^{-/-}$ MEFs were analyzed for expression of SASP gene mRNAs by qRT-PCR. Transcription of these SASP genes in senescent MEFs is also dependent on C/EBPβ (9). n = 3, each sample assayed in triplicate; error bars represent SD; *p < 0.05. **C**, Oncogenic RAS converts KSR1 from a dispersed cytoplasmic distribution to a tightly perinuclear pattern in MEFs. The cells were immunostained using a KSR1 antibody. **D**, Interaction of C/EBPβ with KSR1 is stimulated by HRAS^{G12V} signaling and is inhibited by the *Cebpb* 3′UTR. 293T cells were transfected with C/EBPβ vectors lacking or containing the 3′UTR and pyo-tagged KSR1, ± HRAS^{G12V}. Lysates were immunoprecipitated using a pyo antibody and probed for C/EBPβ and KSR1. **E**, Perinuclear compartmentalization of CK2α and p-ERK1/2 is induced by HRAS^{G12V} in MEFs and requires KSR1. *WT* and *KSR1*$^{-/-}$ cells were infected with control or HRAS^{G12V} retroviruses and immunostained for CK2α and p-ERK. **F**, GFP-labeled KSR1 displays HRAS^{G12V}-induced perinuclear re-localization in NIH3T3 cells. The GFP-KSR1 fusion construct was stably expressed in control and HRAS^{G12V}-transformed cells.

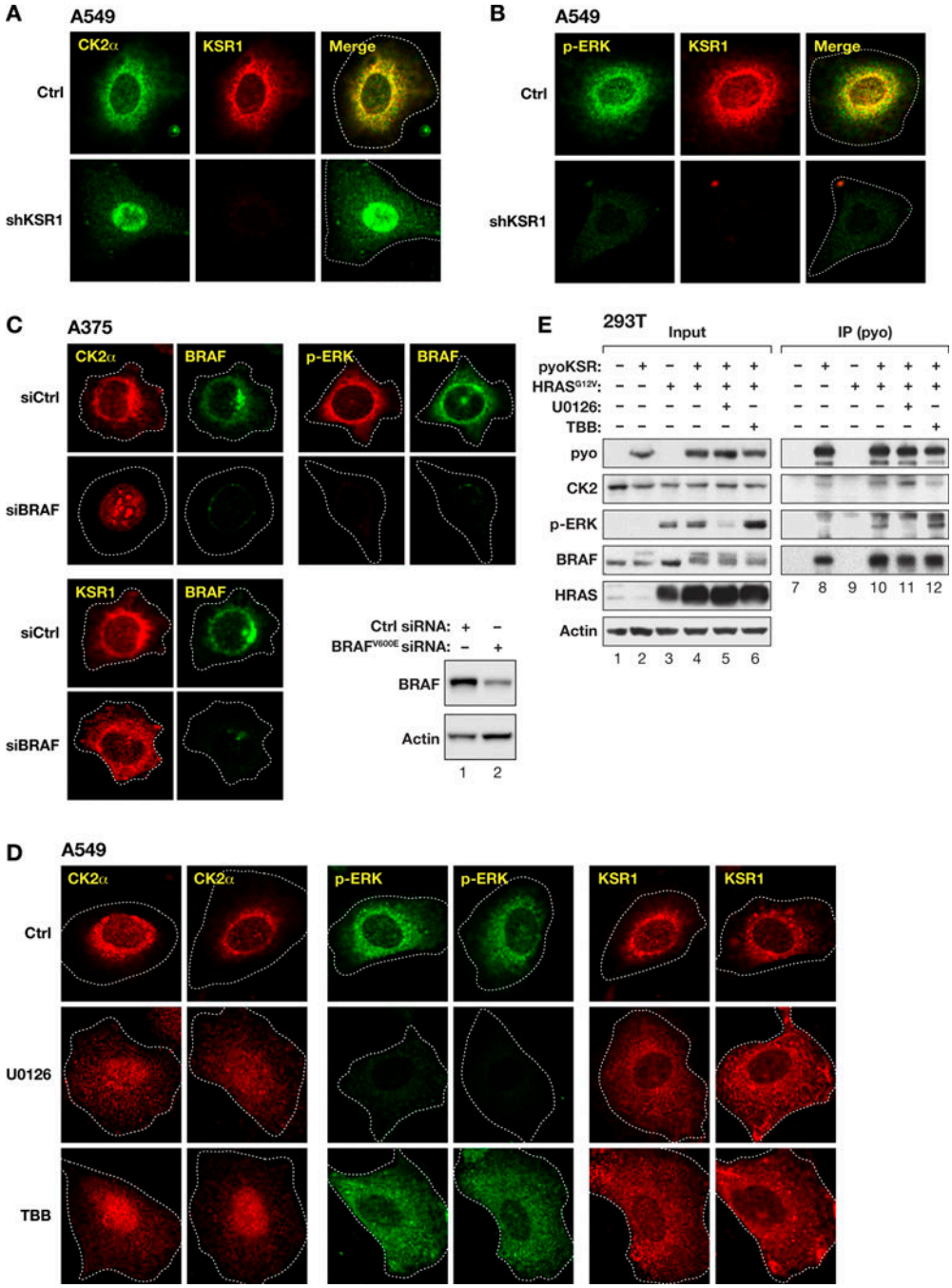

Figure 4.

KSR1-dependent perinuclear signaling complexes are present in human tumor cells and require MEK1/2 and CK2 activity. **A and B**, A549 lung adenocarcinoma cells (*KRAS*^{G12S}) were co-immunostained for CK2α and KSR1 **(A)**, or p-ERK and KSR1 **(B)**, without and with KSR1 depletion using a KSR1-specific shRNA. Cells with efficient KSR1 depletion are depicted. **C**, Human A375 melanoma cells (*BRAF*^{V600E}) display oncogene-dependent perinuclear compartmentalization of RAS pathway signaling complexes. Cells were transfected with control or BRAF^{V600E}-specific siRNAs and immunostained for CK2α, p-

ERK or KSR1, together with BRAF. Cells showing efficient BRAF depletion (low BRAF IF signals) are depicted. BRAF depletion was also verified by immunoblotting (lower right panel). **D**, MEK1/2 and CK2 inhibitors disrupt formation of perinuclear signaling complexes in A549 cells. The cells were treated with vehicle (Ctrl), 5 μM U0126 (MEK inhibitor) or 10 μM TBB (CK2 inhibitor) for 16 hr and immunostained for CK2α, p-ERK1/2, or KSR1. Two examples are shown for each cell population. **E**, Analysis of KSR1-associated signaling complexes in 293T cells. Cells were transfected with Pyo-tagged KSR1 alone or together with $HRAS^{G12V}$. Lysates were immunoprecipitated with a Pyo antibody and the bound fraction was analyzed by immunoblotting for the indicated proteins (lanes 7-12). Cells co-expressing KSR1 and $HRAS^{G12V}$ were also treated with U0126 (5 μM) (lanes 5 and 11) or TBB (10 μM) (lanes 6 and 12) for 16 hr prior to harvest. Input levels are shown in lanes 1-6.

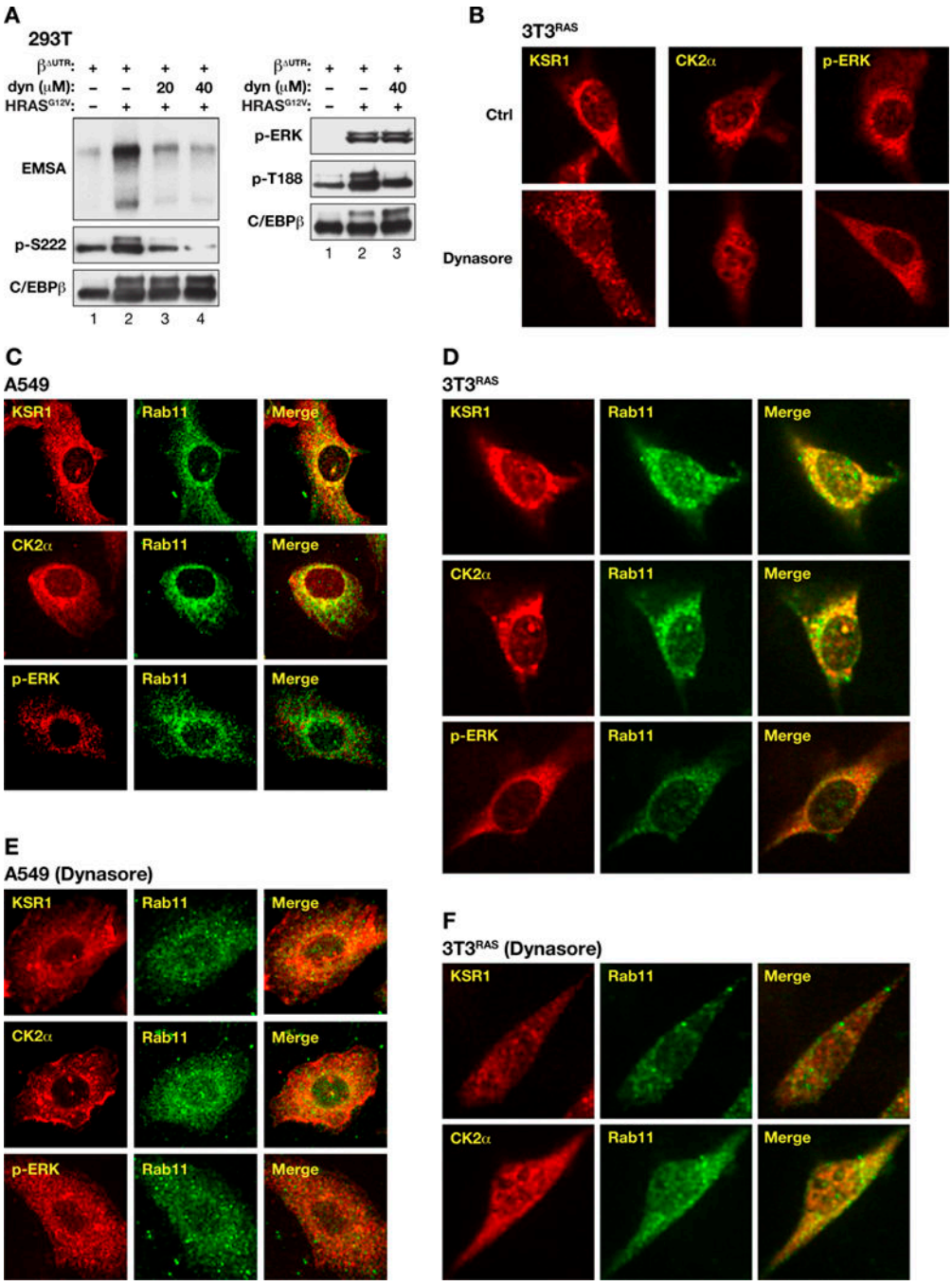

Figure 5.

RAS-induced activation of C/EBPβ and formation of perinuclear signaling complexes requires endocytosis and involves Rab11^{+} endosomes. **A**, 293T cells were transfected with C/EBPβ$^{\Delta UTR}$ plasmid ± HRAS^{G12V} and then treated with vehicle or the indicated concentrations of the dynamin inhibitor, dynasore, for 16 hr prior to harvest. Nuclear extracts were equalized for C/EBPβ levels and DNA binding was assessed by EMSA. The lysates were also analyzed for C/EBPβ phosphorylation by immunoblotting using the indicated antibodies. **B**, Dynasore disrupts perinuclear localization of signaling complexes in

NIH3T3^{RAS} cells. Cells were treated with vehicle or 40 μM dynasore for 16 hr prior to fixation and immunostaining for KSR1, CK2α, or p-ERK1/2. **C**, KSR1 and CK2α partially overlap with Rab11-positive endosomes in A549 cells. Cells were co-immunostained for Rab11 and KSR1, CK2α, or p-ERK. Merged images show appreciable co-localization of Rab11 with KSR1 and CK2α but much less with p-ERK. **D**, Co-localization of Rab11 with signaling proteins is observed in NIH3T3^{RAS} cells. The cells were immunostained as described in panel **C**. **E**, Dynasore prevents perinuclear compartmentalization of CK2α, KSR1 and p-ERK in A549 cells and disrupts co-localization of Rab11 with CK2α and KSR1. Cells were treated with 80 μM dynasore for 16 hr prior to fixation and immunostained for the indicated proteins. **F**, NIH3T3^{RAS} cells were treated with dynasore (40 μM for 16 hr) and co-immunostained for Rab11 and KSR1, CK2α, or p-ERK.

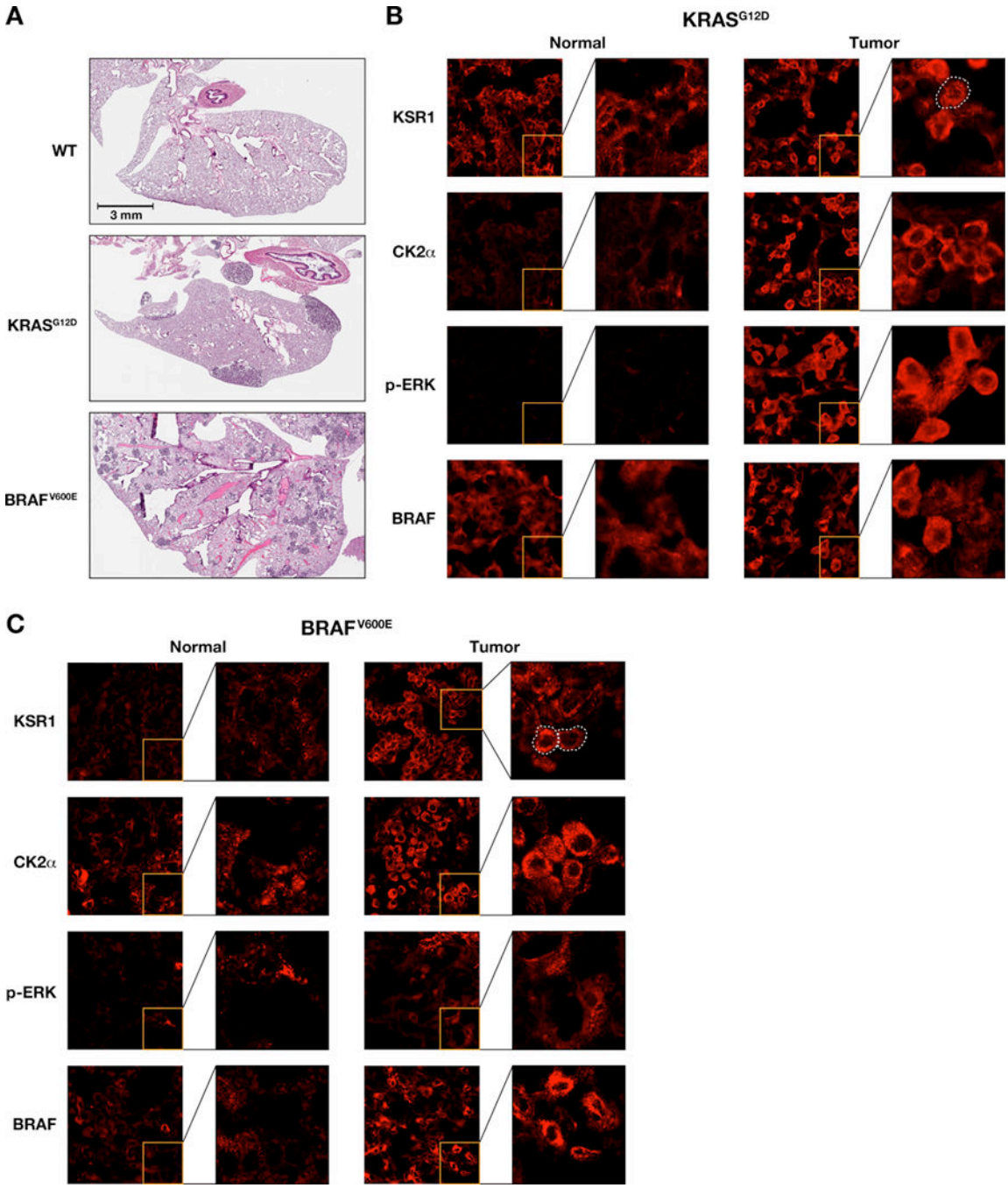

Figure 6.

PSCs are present in *KRAS*^{G12D}-driven mouse lung adenocarcinomas and *BRAF*^{V600E}-induced adenomas. **A**, H&E stained lung sections from *WT* mice and *Kras*^{G12D}- and *Braf*^{V600E}-induced models of lung cancer. **B**, IF staining of normal and tumor-bearing lung areas from *K-ras*^{LA2} mice (22). Frozen sections were immunostained for KSR1, CK2α, p-ERK and BRAF. The tumor images were taken from boundary regions, where the tumor cells are less densely packed and both normal and cancerous cells are visible. A representative KSR1-stained cell is outlined to indicate the cell boundary. **C**, IF staining of

normal and tumor-bearing lung areas from mice carrying *Braf*^{V600E}-induced adenomas (23). Frozen lung tissue sections were immunostained for KSR1, CK2α, p-ERK and BRAF.

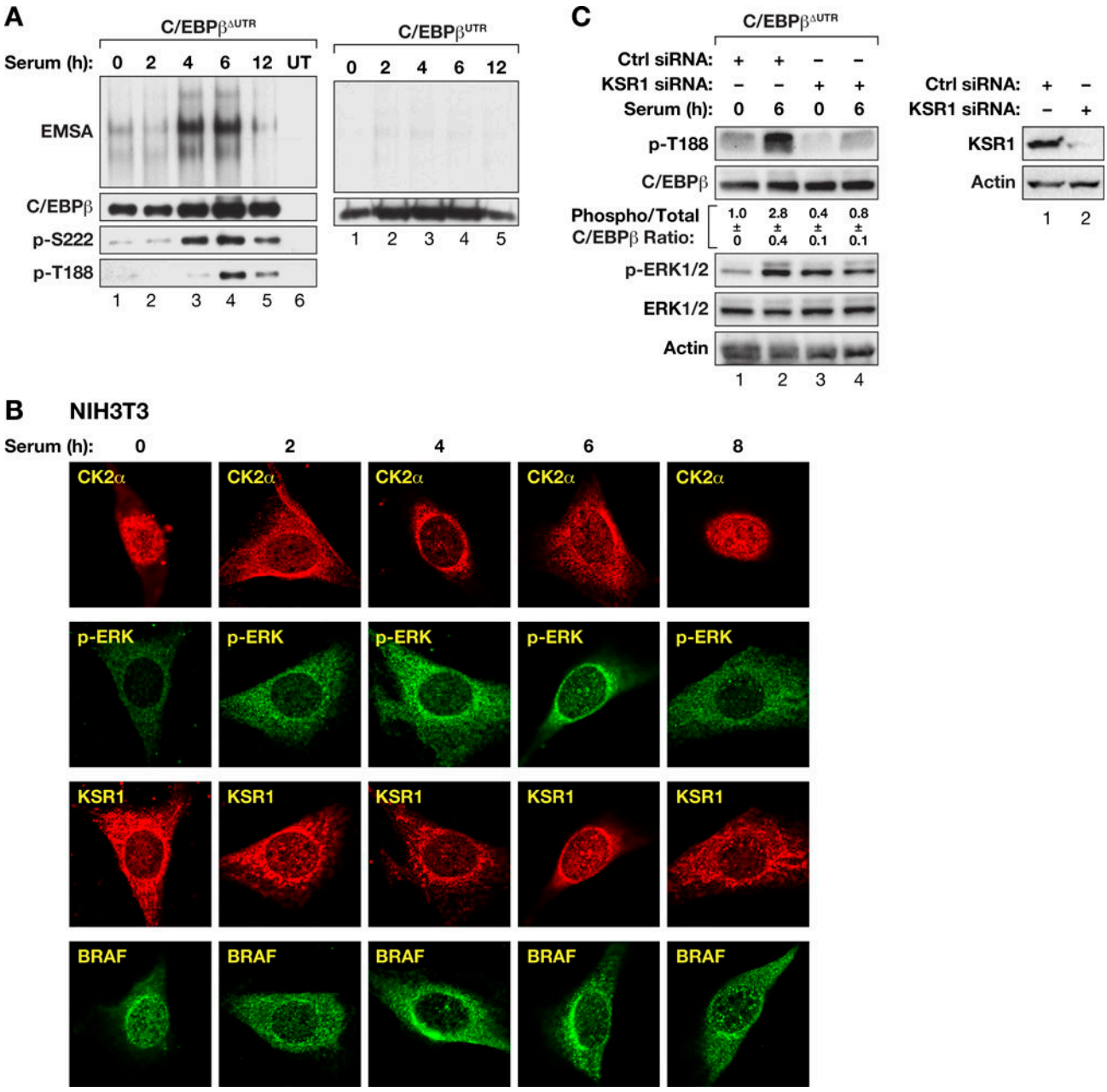

Figure 7.

PSCs form transiently 4-6 hours after GF stimulation in non-transformed cells and correlate with C/EBPβ phosphorylation and activation of DNA binding. **A**, NIH3T3 cells were transfected with plasmids expressing *Cebpb*$^{\Delta UTR}$ (left) or *Cebpb*^{UTR} (right), serum-starved for 24 hr and re-stimulated with serum for the indicated times. Nuclear extracts were prepared and analyzed for C/EBPβ DNA binding by EMSA and immunoblotted for p-S222 (CK2 site), p-T188 (ERK site) and total C/EBPβ. UT, untransfected cells. **B**, PSCs are induced by serum growth factors in NIH3T3 cells with delayed kinetics. Cells were starved, stimulated with serum for the indicated times and immunostained for CK2α, p-ERK, KSR1, or BRAF. **C**, GF-induced phosphorylation of C/EBPβ Thr188 requires KSR1. *Cebpb*$^{\Delta UTR}$-

transfected cells, without or with siRNA-mediated depletion of KSR1, were starved and re-stimulated with serum for 0 or 6 hr and lysates analyzed for C/EBPβ p-T188, total C/EBPβ, and p-ERK. Ratios of p-T188 to total C/EBPβ were calculated from the chemiluminescent images and are shown below the upper panel; n = 2; error represents SD.